REVIEWS OF TOPICAL PROBLEMS

PACS numbers: **52.20.–j**, **52.38.–r**, **52.70.–m**

Spectra of hollow ions in an ultradense laser plasma

I Yu Skobelev, A Ya Faenov, T A Pikuz, V E Fortov

DOI: 10.3367/UFNe.0182.201201c.0049

Contents

Abstract. Experiments with an ultrahigh-contrast femtosecond laser have yielded a new type of X-ray emission spectra with a complex structure consisting of resonance lines against the quasicontinuous background. Some recent work has shown that such spectra can only be accounted for by considering the radiation emitted by multiply charged hollow (empty K shell) ions in an ultradense plasma. This review discusses the observation of the spectra of hollow ions in an ultradense laser plasma and considers the types of such ions and how they are excited. Considerable opportunities of hollow ion spectra-based diagnostic techniques are emphasized.

1. Introduction

The X-ray emission spectra of plasmas produced by nano- and subnanosecond laser pulses have been vigorously investigated for more than 40 years (see, for instance, Refs [1–8]). In particular, the spectral characteristics of the radiation in the vicinity of the resonance lines of H- and He-like multiply charged ions have been studied in sufficient detail. The typical structure inherent in the spectra of this domain is characterized by the presence of groups of satellite spectral lines (dielectronic satellites) arising from radiative transitions from ion autoionization states (Fig 1a). This structure is adequately described by collisional-radiative kinetics (see, for instance, Refs [1–6]) which employ the theoretical values of atomic characteristics (energy levels, the probabilities of elementary atomic processes). The diagnostic properties of these spectra, which rely on the relative line intensities and spectral line profiles, are generally known and are widely used for determining the parameters of laboratory (laser plasmas, tokamaks, Z- and X-pinches, etc.) and astrophysical plasmas (see, for instance, reviews [1–6] and references cited therein).

The X-ray emission of plasmas produced by pico- and subpicosecond lasers has become the subject of different investigations in recent years. The spectral features of this emission have much in common with those previously observed in experiments with longer laser pulses. The measured spectra are rather conventional in shape (Fig. 1b), which is reproduced quite well by a quasistationary collisional-radiative model, while the changes in line intensities are described by the variations of such plasma parameters as the temperature, the density, the optical thickness, and the ionization composition (see, for instance, Refs [9–16]). Accounting for certain differences from the emission spectra of nanosecond laser plasmas requires introducing hot electrons into the kinetic model, as well as taking into consideration that the preplasma produced by a laser prepulse plays a significant part in the interaction of short laser pulses with matter [17–22].

Experiments carried out with a femtosecond laser characterized by an ultrahigh contrast (the pulse-to-prepulse intensity ratio) of the order of 10^{11} [23, 24] enabled recording for the first time spectra of a new type, which had not been observed in the X-ray wavelength range (Fig. 1c). The emergence of the spectra of a new type unambiguously evidenced that the change-over to an ultrahigh laser contrast is accompanied by radical changes in the parameters of a generated plasma.

The observed 'unusual' spectra are distinguished from the more ordinary ones by the presence of a complex quasicontinuous structure, with the principal lines embedded into it. The theoretical spectra calculated using the coronal quasistationary kinetic plasma model [1] (Fig. 1d), which resemble the

I Yu Skobelev, V E Fortov Joint Institute for High Temperatures, Russian Academy of Sciences,
ul. Izhorskaya 13, str. 2, 125412 Moscow, Russian Federation
E-mail: igor.skobelev@gmail.com, fortov@ihed.ras.ru
A Ya Faenov, T A Pikuz Joint Institute for High Temperatures, Russian Academy of Sciences,
ul. Izhorskaya 13, str. 2, 125412 Moscow, Russian Federation
E-mail: anatolyf@hotmail.com
Quantum Beam Science Directorate, Japan Atomic Energy Agency, Kyoto, Japan

Received 19 April 2011, revised 10 June 2011
Uspekhi Fizicheskikh Nauk **182** (1) 49 – 75 (2012)
DOI: 10.3367/UFNr.0182.201201c.0049
Translated by E N Ragozin; edited by A Radzig

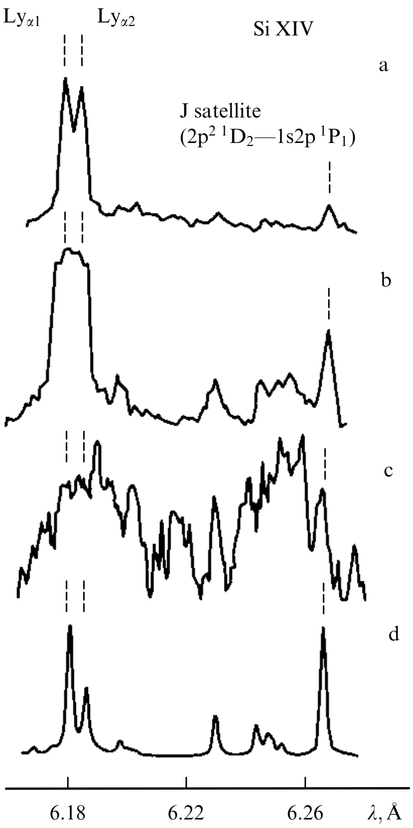

Figure 1. Emission spectra of silicon plasma heated by nanosecond (a) [3], low-contrast (b) [9], and high-contrast (c) [23] subpicosecond laser pulses in the vicinity of the Ly$_\alpha$ resonance line of H-like Si XIV ions. The theoretical spectrum (d) corresponds to a coronal model.

experimental spectra examined earlier, turned out to be utterly unsuitable for describing the new type of spectra.

Of course, the physical reason for so drastic a restructuring of the spectrum lies with the difference in plasma production mechanisms. The absence of a preplasma secured the direct interaction of ultrashort laser pulses with solid material, resulting in the production of plasma possessing and a substantially higher electron density, on the one hand, and a huge spatial density and temperature gradients, on the other. Under these densities, the plasma emission spectrum comes to be dominated by a plethora of spectral lines which are hardly excited in a uniform coronal plasma.

As shown in Refs [23–26], the new type of observed spectra may be interpreted only by way of inclusion of the radiation emitted by multiply charged hollow ions (i.e., by ions with an empty K shell) in an ultrahigh-density plasma. Radiative transitions of this type in neutral and quasineutral objects (hollow atoms), which were observed in experiments on the interaction of ion beams (see, for instance, Refs [27–36]) or synchrotron radiation (see, for instance, Refs [37–40]) with solid surfaces, have been under active scrutiny over the last two decades. Similar structures for multiply charged ions were presumably observed for the first time in the spectra arising from close-to-target regions in the plasma produced by the nanosecond pulse of the Nike laser (Naval Research Laboratory, USA) [41].

Like ordinary spectral lines, spectra of the new type, i.e. those of hollow ions, offer considerable diagnostic opportunities. At the moment, ample realization of these opportunities is hindered by the absence of systematic precision atomic calculations of hollow structures. It is noteworthy that there are supposedly no difficulties of a fundamental nature in this case. It is simply that such calculations have not been called for until recently.

A very strong incentive for the development of theoretical and experimental spectroscopy of hollow ions is that the new type spectra should be excited in warm dense matter and in nonideal plasmas [42–51]. As shown in Sections 2–4, these spectra are radiated in the electron transitions between deep inner ion shells, and therefore nonideality effects, which are very hard to calculate quantitatively, will have only a moderate effect on the spectra of hollow ions. This signifies that the spectra of hollow ions may be applied to the X-ray spectral diagnostics of nonideal plasmas without any modifications.

In this review we discuss the observations of hollow-ion spectra in ultrahigh-density laser plasmas and consider the types of hollow ions and the mechanisms of their excitation. Emphasized is the great urgency of hollow ion investigations in connection with the emergent possibility of harnessing the radiation of high-power X-ray lasers for plasma production.

2. What hollow ions are and where their spectral lines lie?

2.1 Autoionization states and hollow-ion states

In the foregoing we mentioned that hollow ions are those with an empty inner electron shell. Let us consider their structure in more details. Recall that a hydrogen-like ion, i.e. the ion with one electron (and an arbitrary nuclear charge Z_{nucl}), can occupy the ground state (1s) and the resonance level (2p) (i.e., the first excited level which is connected with the ground state by an allowed radiative transition). Accordingly, the resonance line of the hydrogen-like (H-like) ion is the Ly$_\alpha$ line arising from the 2p–1s transition.

Now let us add one electron to the L shell (i.e., a 2s or 2p electron) of the excited state of these ions. We obtain a doubly excited state of the 2p^2 or 2s2p type (hereinafter both of these states will be denoted as $2l^2$ for simplicity), which is, in addition, an autoionization state, since its energy exceeds the ionization energy. The radiative decay of this state will result in the emission of the $2l^2 - 1s2l$ spectral line, which is somewhat longer in wavelength than the resonance line of the H-like ion discussed above: the transition of the optical electron now occurs in the Coulomb potential of a $Z_{\mathrm{nucl}}^{\mathrm{eff}}$ nucleus partly screened by the additional electron: $Z_{\mathrm{nucl}}^{\mathrm{eff}} < Z_{\mathrm{nucl}}$. This line is referred to as the dielectronic satellite of the resonance line of the H-like ion. In reality, the $2l^2$ and $1s2l$ electron configurations make up several ionic terms rather than one, so that we are dealing with a whole group of satellite lines rather than with one satellite line. We also emphasize that the dielectronic satellites of the resonance line of an H-like ion are transitions in a two-electron ion, i.e., in an He-like ion.

If we now add another excited electron, we shall obtain a triply excited Li-like ion state ($2l^3$). This state is also an autoionization one, and its radiative decay, $2l^3 - 1s2l^2$, will produce spectral lines shifted to the long-wavelength side of the satellites discussed above. These lines, which are hypersatellites, i.e. the satellites of satellites, result from transitions in hollow ions. The hollow ions themselves are ions occupying the $2l^n$ states. Formally, the $2l^2$ state is also

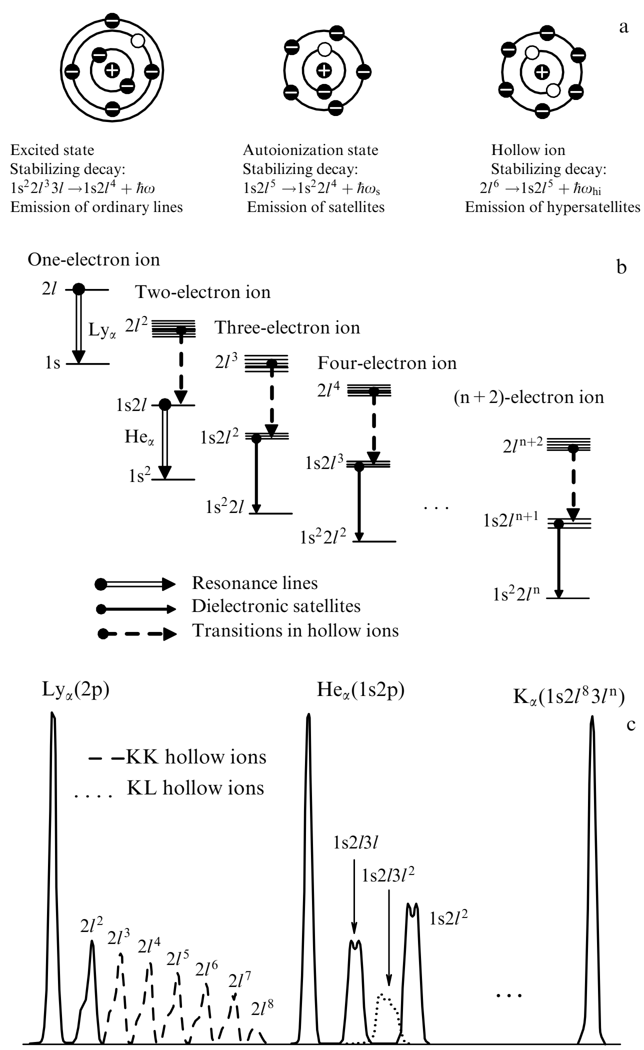

Figure 2. (a) Electron shell structure of excited, autoionization, and hollow ion states. (b) Energy level diagram for ordinary, autoionization, and hollow ion states with valence K and L shells. (c) Approximate positions of the Ly_α resonance line of an H-like ion, the resonance He_α line of an He-like ion, the characteristic K_α line, dielectronic satellites ($2l^2$, $1s2l^2$, $1s2l3l$), and hypersatellites (the lines of hollow ions) in the ion emission spectrum; the electron configurations of the upper levels of spectral transitions are indicated for all lines; the location of the dielectronic satellites and hypersatellites with the number of electrons greater than three is marked with ellipsis.

the state of a hollow ion, since it has two electrons in the outer L shell, and an empty inner K shell. However, the radiative decay of this ion state gives rise to satellite transitions of the resonance line itself rather than to transitions of the satellites to another satellites. That is why we shall not refer to the states of this type as to those of hollow ions. It is pertinent to note that these state have been comprehensively studied for the last 50 years and the data on them may be found in Refs [1–5, 52–54].

All the aforesaid may be illustrated by Fig. 2, which conventionally shows the electron shell structures of excited, autoionization, and hollow ion states (Fig. 2a), as well as the energy level diagrams of these states (Fig. 2b). Figure 2c displays the approximate relative positions of the resonance line, the dielectronic satellites, and the hypersatellites in the ion emission spectrum.

2.2 Types of hollow ions

Hollow ions, as discussed in Section 2.1, have two holes in the inner K shell. This is the most obvious type of hollow ion, which is naturally termed the KK or K^2 hollow ion. At present, other types of hollow ions are also considered. For instance, a state with two vacancies in the L shell is also reckoned to be among hollow ions when at least one higher-shell (M, N, etc.) electron is present. Such a hollow ion is termed the L^2 hollow ion. Mixed types of hollow ions may also occur, for instance, a KL hollow ion having a one-electron vacancy in each of the K and L shells. The number of vacancies may be greater, and in this case we are dealing with $K^n L^m$ hollow ions.

Therefore, the ion states with one inner-shell vacancy are commonly referred to as autoionization states, and the ion states with two vacancies as the states of hollow ions. Of course, implied in all of these cases is the presence of at least one electron in a higher energy shell. The radiative decay of the autoionization states results in the emission of satellites, and the radiative decay of the states of hollow ions is accompanied by the emission of hypersatellites. Below we shall use precisely this terminology, which is becoming progressively more conventional. It should be emphasized that since we do not put $2l^2$ type states into the category of K^2 hollow ions, the $1s2l^m nl$ states will not be treated as KL hollow ions, either. The radiative decay of these states results in the emission of so-called Rydberg satellites, whose properties have been studied in sufficient detail (see, for instance, Refs [1–5, 55–65]).

2.3 Spectral domains containing the hollow-ion lines

The main qualitative rules for the location of hollow-ion spectral lines relative to the corresponding resonance lines and satellites were mentioned in Section 2.1 (see the conventional diagram in Fig. 2c). Of course, quantitative determination of the hypersatellite wavelengths requires carrying out detailed atomic calculations for isolated ions with the inclusion of relativistic effects, a start on which has recently been made; however, information is still scarce. By contrast, the calculations of satellite wavelengths have been underway for several decades, and a wealth of information, both theoretical and experimental, has been acquired in this area. This information may be employed for prompt quantitative estimates of hypersatellite wavelengths, which prove to be helpful in the arrangement of experiments to observe hypersatellites, as well as in the identification of hollow-ion spectra.

Let us endeavor to estimate, for instance, the positions of the $(2l)^k(3l)^m(4l)^n\ldots - 1s(2l)^{k-1}(3l)^m(4l)^n\ldots$ transitions in magnesium KK hollow ions [66].

The resonance Ly_α doublet of H-like Mg XII ions has an average wavelength of 8.421 Å, and the He_α resonance line of Mg XI ions has a wavelength of 9.1697 Å. Calculations [67, 68] of the dielectronic satellites of these lines reveal (and this is in perfect agreement with experimental data) that the addition of one electron to the $2l$ shell shifts the 2p–1s optical electron transition wavelength by 0.13–0.25 Å owing to the partial screening of the Coulomb nuclear field. An electron added to the $3l$ shell screens the nucleus considerably more weakly, and the satellite wavelengths shift by 0.02—0.04 Å. For a $4l$ electron, the shift is even smaller: 0.01–0.02 Å. This signifies that the $2l$ electron lowers the effective charge of the atomic core by 0.092, the $3l$ electron by 0.02, and the $4l$ electron by 0.007. (Needless to say, here we are dealing with the effective charge experienced by the optical electron; the screening parameter for higher-excited optical electrons will be larger.) Hence, it follows that the $(2l)^k - 1s(2l)^{k-1}$ transitions for $2 \leqslant k \leqslant 6$, i.e. transitions in He-, Li-, Be-, B-, and C-like hollow ions supposedly lie in the 8.42–9.17 Å wavelength range under consideration. Furthermore, since the shifts caused by higher-excited orbitals are significantly smaller, this will also be the location of the $(2l)^k(3l)^m(4l)^n\ldots - 1s(2l)^{k-1}(3l)^m(4l)^n\ldots$. transitions in hollow ions with a greater number of electrons.

From qualitative estimates of this kind it follows that one more class of spectral lines may overlap with the spectra of magnesium hollow ions. These are the lines arising from the electron optical transitions from the state with the principal quantum number $n' = 3$ to states with the principal quantum number $n = 1$. Specifically, the wavelength of the $1s3p–1s^2$ transition in He-like Mg XI is equal to 7.8508 Å. Therefore, on the addition of four or more electrons to the $2l$ shell the total spectral shift would be sufficiently large for the transitions to fall into the spectral range of interest. Adding several more electrons to higher-excited shells ($3l, 4l, \ldots$) does not change the situation, and we draw the conclusion that the 8.42–9.17 Å wavelength range should contain the transitions

$$1s(2l)^{n_2}(3l)^{n_3}(4l)^{n_4}\ldots - (1s)^2(2l)^{n_2}(3l)^{n_3-1}(4l)^{n_4}\ldots$$

with $n_2 \geqslant 5$. It is noteworthy that not all of these transitions represent transitions in hollow ions, since a part of them are the dielectronic satellites of the He_β line of the He-like ion, which arise from the radiative decay of autoionization states in relatively low-ionized N-, O-, F-, Ne-, Na, and Mg-like magnesium ions. These satellite lines have not been observed to date. This is due to the following fact. To efficiently excite them requires, on the one hand, a sufficiently cool plasma with a temperature of no higher than several dozen electron-volts (otherwise the plasma will be void of ions with so low a charge multiplicity) and, on the other hand, the presence of kilo-electron-volt electrons capable of exciting the satellite transitions. It is very hard to simultaneously meet both of these requirements in a laser plasma. The lines indicated above may supposedly be observed in the heating of solid targets by high-power electron beams, but such experiments, to the best of our knowledge, have never been carried out. Similarly, the satellites of the lines He_γ, He_δ, etc. may also fall into the spectral range under consideration for the greatest possible number of screening electrons (neutral and singly or doubly ionized magnesium). But the intensities of these lines should be still lower and their recording is a more complicated task.

The qualitative estimates made above are borne out by numerical calculations of the atomic structure of magnesium ions performed in Ref. [66]. The results of these calculations, along with the data of numerical calculations of the spectra of other hollow ions, will be outlined in Sections 3 and 4 in the discussion of the observations of hollow-ion spectra in ultrahigh-density laser plasma and of their simulation data.

It is pertinent to note that the term 'ultrahigh-density laser plasma' applies, strictly speaking, to a laser plasma with an electron density exceeding the critical value for the wavelength of its generating radiation. However, since the most popular laser systems used for plasma heating are those with a wavelength of about 1 μm, which corresponds to a critical electron density of 10^{21} cm^{-3}, the term 'ultrahigh-density' is commonly employed in reference to laser plasmas with $N_e > 10^{21}$ cm^{-3}. In what follows we shall adhere to precisely this terminology, while the term 'dense' will be applied to plasmas with $N_e \sim 10^{19} - 10^{21}$ cm^{-3}.

3. Mechanisms of hollow-ion excitation in inhomogeneous plasma

For a considerable amount of hollow ions to emerge in a plasma, a mechanism is required to ensure an efficient removal of inner-shell electrons without ionizing the outer shells. Strictly speaking, such a mechanism does not exist, but we can endeavor to find processes whereby the probability of removing inner-shell electrons is at least not too small in comparison with the probability of outer-shell ionization. Generally speaking, ionization in plasmas may take place in the collision of an ion with electrons, other ions, or photons.

In ion–ion collisions, both nonresonance ionization by the Coulomb field of the impinging ion and resonance charge exchange are possible. The former process in a plasma may be neglected because the cross sections for ionization by ion impact are large only for ultrahigh ion energies attained only in accelerators [7]. It is noteworthy that the first observations of the spectra of hollow atoms (a hollow atom is the special case of a hollow ion with a zero total charge) were nevertheless made in precisely the accelerator experiment [27]. The resonance charge exchange mechanism may excite the states of hollow ions, which calls for the interaction of ions with substantially different charge multiplicities. This may be realized, for instance, when a laser plasma expands into a gas medium (see Section 4.1.3).

Ionization processes in a plasma proceed most often due to electron impact. In this case, the electron energy must also be rather high in comparison with the inner-shell ionization energy, but nevertheless lower than in the case of ion-impact ionization. For ions with charges of about 10 it would suffice to have electrons with energies of several kiloelectronvolts, and, as is commonly known (see, for instance, Refs [69–74]), such electrons are generated in sufficient quantities in plasma production by subpicosecond laser pulses at flux densities above 10^{16} W cm^{-2}.

Hot electrons may produce hollow ions, but do so with not-too-high efficiency. Indeed, the electron impact ioniza-

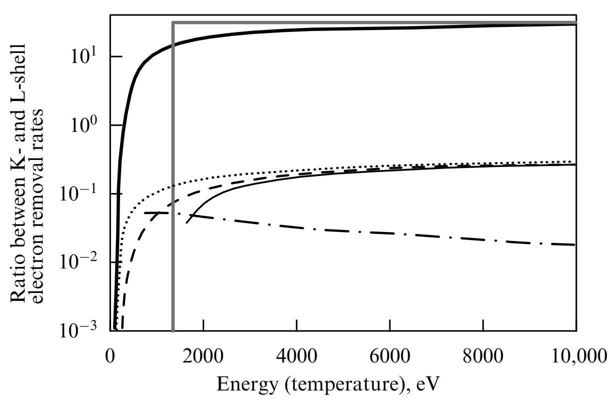

Figure 3. Ratios between the probabilities of photon-induced electron removal from the K and L shells of the ion with $Z = 10$ (grey and dark solid bold lines) and those induced by electrons (the remaining curves) as functions of their energy or temperature. The grey bold line stands for a monochromatic X-ray source, and the dark bold line stands for blackbody radiation. The thin solid curve stands for a monochromatic electron beam, the dashed curve for ionization by Maxwellian electrons, the dashed-dot curve for excitation by Maxwellian electrons, and the dotted curve is the net result of ionization and excitation by Maxwellian electrons.

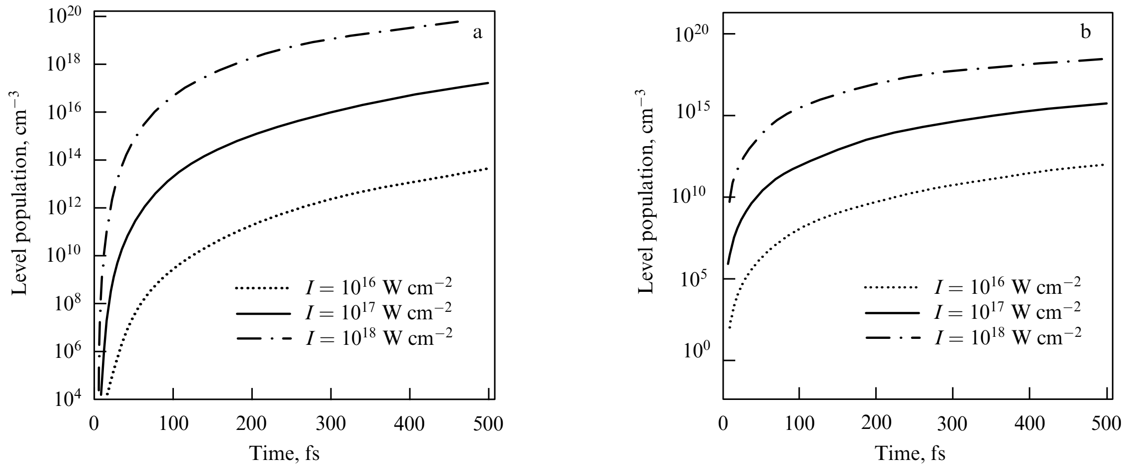

Figure 4. Time dependences of the autoionization (a) and hollow-ion (b) state populations for different intensities of laser radiation [75].

tion rates are approximately proportional to n^3, where n is the principal quantum number of the electron being ionized. Hence, it follows that a hot electron will ionize the L shell with a much higher probability (by nearly an order of magnitude) than the K shell (Fig. 3). Therefore, K^2 hollow ions will be produced in the collisions of ions with hot electrons, but in far lower numbers than ordinary ions. This conclusion is practically independent of whether the hot ions are monoenergetic (an ion beam) or thermal, as is evident from Fig. 3. Broadly speaking, hollow ions may be produced not only by way of inner-shell ion ionization, but also due to the excitation of an inner electron and its transition to an outer shell. However, the situation is hardly changed on inclusion of this process (see the dashed and dotted curves in Fig. 3).

The case with KL, L^2, LM, etc. hollow ion production is somewhat better. Here, the ratio between electron-impact ionization rates for neighboring shells will be closer to unity and the amount of hollow ions may be quite significant.

Therefore, even from simple estimates it follows that the presence of hot electrons in plasmas may result in the excitation of hollow ions, but the population of these states will not be high. The same conclusion is drawn from detailed kinetic calculations. For instance, a kinetic model corresponding to the case of interaction of a 500-femtosecond laser pulse with a solid magnesium target at intensities of $10^{16}-10^{18}$ W cm^{-2} was considered in Ref. [75]. In this model, the K and L inner electron ionization resulted both from collisions with a hot electron and from autoionization processes. Also included was the transition of an excited inner electron to an outer shell, resulting in the production of a hollow ion. The hot electrons were assumed to have the following velocity distribution function

$$N_{\mathrm{h}}(v) = \sqrt{\frac{8m}{c^2}}\,\frac{\eta}{T_{\mathrm{h}} - (T_{\mathrm{h}} + E_{\mathrm{c}})\exp(-E_{\mathrm{c}}/T_{\mathrm{h}})} \times \exp\left(-\frac{mv^2}{2T_{\mathrm{h}}}\right), \tag{1}$$

where T_{h}, E_{c}, and η are approximation parameters, which in accordance with Refs [76, 77] were taken as follows: $T_{\mathrm{h}} = 30I^{1/3}$, where I is the flux density of a laser pulse in units of [10^{17} W cm^{-2}], $E_{\mathrm{c}} = 4T_{\mathrm{h}}$, and $\eta = 0.3$.

A nonstationary kinetic problem was solved, with all ions being in the ground state of Ne-like Mg at the initial point in time. The results of simulation are shown in Fig. 4 for three intensity values of a laser pulse. One can see that the hollow-ion level population increases approximately as I^3 relative to the population of autoionization levels, but even for $I = 10^{18}$ W cm^{-2} it amounts to only about 1%.

The case is quite different in the interaction of an ion with an X-ray photon, where the electron removal cross section (the photoionization cross section) is approximately proportional to n^{-5}, i.e., the photon incident on the ion will remove electrons with overwhelmingly high probability from the innermost shell whose ionization energy does not exceed the photon energy. By way of example, Fig. 3 depicts schematically the ratio between the probabilities of electron removal from the K and L shells of an H-like ion with $Z = 10$ for the photoionization by monochromatic radiation (grey curve) and by blackbody radiation (dark bold curve). One can clearly see that it is precisely the K^2 hollow ion production which is the prevailing process, when the photon energy is, of course, high enough. For instance, the photon energy must exceed the K-shell ionization potential when use is made of monochromatic radiation; when use is made of the radiation of a blackbody, its temperature must be higher than one fourth of the K-shell ionization potential.

X-ray radiation capable of producing hollow ions may be emitted by the plasma itself. This effect should be most pronounced when the plasma is strongly inhomogeneous and there are regions with substantially different temperatures. In this case, the radiation generated in the hot region will produce hollow ions in the cold region where the electron temperature is not high enough to ionize the ion outer shells.

At present, the process of hollow ion production by X-ray radiation is becoming more topical in connection with the advent of high-power X-ray lasers, both plasma-based and free-electron lasers [7, 42, 78–80]. With such lasers, the very energy input process, unlike that in the case of interaction of optical laser radiation with matter, is directly related to hollow ion production. Recall that the major part of the energy of a substance-irradiating optical laser pulse is initially spent to heat the emerging free electrons. And only later, in electron–ion collisions, the energy is imparted to ion internal energy (collisional ionization and production of multiply charged ions), and subsequently into the ion kinetic energy. By contrast, in the absorption of an X-ray photon the major part of energy may immediately go into the internal energy of emerging autoionization and hollow-ion states, and only then will a part of it be transferred to the free plasma electrons in the course of autoionization. In this case, plasma production process will depend heavily on the ratio between the X-ray laser photon energy and the ionization potentials of various atomic shells of the target material. In this connection, it should be mentioned a very interesting experiment [81] on the absorption of high-power X-ray radiation by aluminium foil.

The interaction of sufficiently intense monochromatic X-ray radiation with targets may give rise to target self-bleaching wherein the target ceases to absorb the radiation and becomes almost transparent in the course of heating. In the simplest (and the least interesting) case this may be due simply to the complete ionization of target atoms to the state of bare nuclei, which is of course possible but requires high fluences. Owing to the production of hollow ions, however, this effect may occur for substantially lower energy inputs. As noted above, the inner K-shell photoionization cross section far exceeds the L-shell photoionization cross section (and even more so that of M, N, ... shells). This signifies that, as soon as the K^2 type hollow ions come to prevail in the plasma, the absorption of photons with energies above the K edge by the target will decrease sharply, i.e. target self-bleaching will occur. In this case, the degree of substance ionization will not be too high, low-charged ions may prevail in the target substance, and substantially lower energy inputs will therefore be required to produce such a state. Naturally, a similar effect may also be achieved for L^8 type hollow ions, but it will be more weakly pronounced, since the difference between the L- and M-shell photoionization cross sections is no longer so significant.

The induced transparency effect is of major practical significance. The execution of X-ray structural investigations of microobjects, including medical and biological ones, calls for exposing these objects to rather high X-ray irradiation doses in order to obtain high-quality diffraction images. However, raising the irradiation dose increases, as a rule, the absorbed dose. This is undesirable, for it may cause damage to the object under study. We note that the typical damage threshold amounts to 200 X-ray photons per Å^2. The self-bleaching effect permits raising the incident fluence with hardly any increase in absorbed fluence [82].

Highly interesting situations may be realized when there is an opportunity to continuously tune the frequency of monochromatic X-ray radiation, i.e. with the use of free-electron lasers [78–80]. Since the energy required for the excitation of the K^1 autoionization state is lower than the energy for the K^2 hollow ion excitation, it is possible to select the X-ray photon energy so that it suffices to generate the autoionization state and is insufficient for producing the hollow ion. We may then obtain a plasma void of hollow ions, and the self-bleaching will take place at the stage of autoionization level excitation. An experiment of this kind was recently reported in Ref. [81].

As noted above, the amount of hollow ions produced by X-ray radiation may be quite large. This follows not only from the simple estimates of photoionization cross sections given above (see also Fig. 3), but also from detailed kinetic calculations. A kinetic model was constructed in Ref. [83] for describing the plasma produced by the radiation of an ordinary optical laser, which was additionally irradiated by an X-ray free-electron laser. To this end, the conventional system of nonstationary kinetic equations was supplemented with terms describing photoionization, stimulated photorecombination, stimulated emission, and absorption. Specific simulations were made for magnesium plasma and a 100-fs-long X-ray pulse. The X-ray photon energy was varied; an electron number density $N_e = 10^{21}$ cm^{-3} and temperature $T_e = 30-50$ eV were specified for the initial plasma state. A typical result of the simulations [83] is demonstrated in Fig. 5, which gives the time-dependent intensities of the Ly$_\alpha$ Mg XII, He$_\alpha$ Mg XI, and K^2 hollow Mg XI and Mg X ion spectral lines for two cases: in the absence of X-ray pumping (Fig. 5a), and with plasma irradiation by 1.2×10^{10} X-ray photons with an average energy of 3100 eV (and an energy distribution width of 6.2 eV) focused on a spot 30 μm in diameter (Fig. 5b). With reference to Fig. 5, it can be seen that in the absence of X-ray pumping the K^2 hollow ions are hardly produced, while in the presence of the pumping the hollow state populations are practically the same as the populations of the resonance levels.

The simulations of Ref. [83] also demonstrated a very interesting time behavior of the degree of plasma ionization. From the onset of X-ray pulse irradiation, the plasma

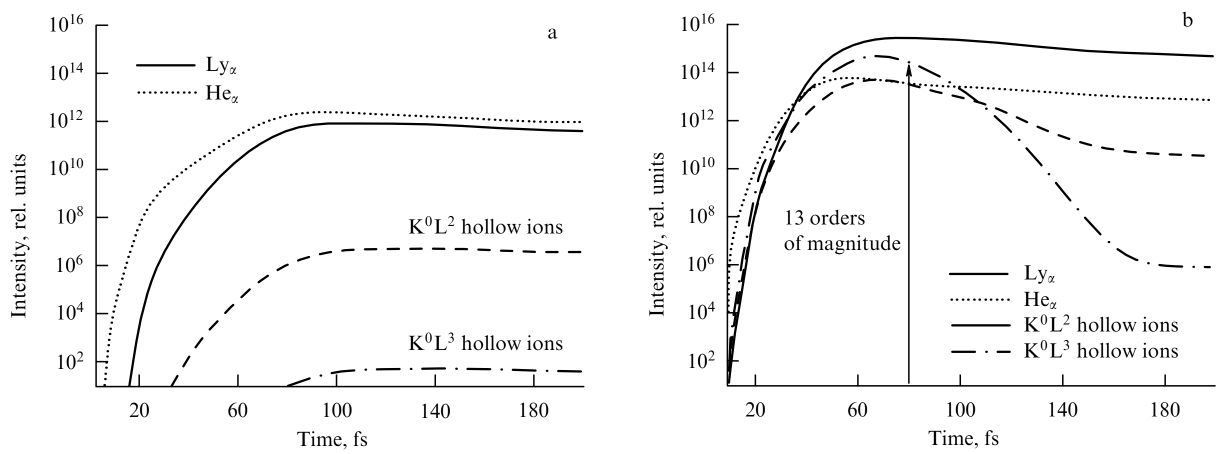

Figure 5. Time dependences of the intensities of the Ly$_\alpha$ Mg XII, He$_\alpha$ Mg XI, and K^2 hollow Mg XI and Mg X ion lines for two cases: (a) X-ray pumping is absent, and (b) 1.2×10^{10} X-ray photons with an average energy of 3100 eV (with a distribution width of 6.2 eV) focused on a spot 30 μm in diameter are incident on the plasma [83].

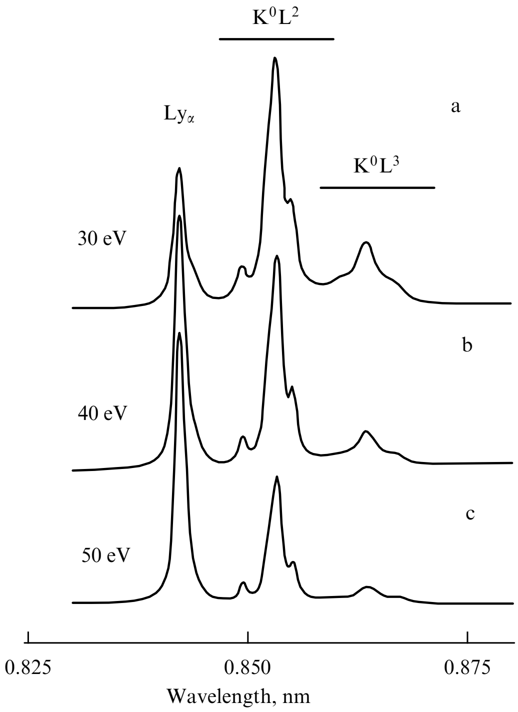

Figure 6. Dependence of hollow ion spectra on the substance temperature according to the simulations performed in Ref. [83].

becomes overionized, with the majority of ions being the bare nuclei of magnesium. The cessation of the X-ray pulse is immediately followed by the stage of recombination, which is relatively long; the emission of ordinary spectral lines is continued during this stage. The emission of hollow ions terminates much earlier (see Fig. 5). By lowering the pumping X-ray photon energy E_{ph} it is possible to ensure the prevalence of some other ions rather than the bare nuclei. For instance, the plasma will be dominated by He-like Mg XI ions at $E_{\text{ph}} = 1850$ eV, while the Mg XIII nuclei will account for less than 0.1%.

Additional plasma exposure to an X-ray photon beam makes it possible not only to observe the spectra of hollow ions, but also to use them for diagnostic purposes. This is most relevant when the state produced by optical laser radiation corresponds to warm dense matter or a nonideal plasma [7, 8, 42–44]. As shown by the simulation data of Ref. [83] given in Fig. 6, the spectra of hollow ions have to depend heavily on the temperature of the matter, which therefore permits its measuring.

The production of hollow ions must play a highly important part in the course of ionization of a medium by the radiation of high-power X-ray lasers, the mechanism of ionization being strongly dependent on the X-ray photon energy. By way of example, consider the ionization of a neon target exposed to X-ray photons of different wavelengths, as was done in Ref. [82].

When the X-ray photon energy is below the neutral neon K-shell ionization threshold (which is equal to 870 eV), the incident X-ray radiation will photoionize the outer (valence) L shell, with the result that we obtain a plasma containing the He-like Ne IX ions. In this case, the only process leading to ionization of the medium is the photoionization of the valence shell.

If the photon energy is raised above 993 eV, other ionization processes begin to participate. Initially, the photoionization of a K electron will occur with the formation of an autoionization state, and then two versions of the progress of events will be possible: either autoionization with the filling of the K-shell vacancy and an L-electron detachment, or another K-electron photoionization with the formation of a hollow ion and the subsequent autoionization. This chain of processes may terminate on the attainment of some ion charge multiplicity, depending on the photon energy, and subsequently only the photoionization of valence electrons will take place. The plasma of Ne IX ions will eventually result again.

When the photon energy exceeds 1360 eV, the chains of ionization processes will proceed to the end, giving rise to the plasma of bare Ne IX nuclei. It is significant that the photoionization–autoionization–photoionization chains, which take place with the participation of the inner ion shells, are a significantly faster process than simply the photoionization of a valence shell [82]. Consequently, in the previous case the same degree of ionization of the substance will be reached in a substantially shorter time.

Quite recently the ionization of a neon target exposed to the pulse of the LCLS (Linac Coherent Light Source) X-ray laser of the SLAC National Accelerator Laboratory, USA was investigated experimentally [82]. The X-ray photon energy was equal to 800, 1050, or 2000 keV in different experiments, for a maximum photon fluence of 10^5 Å^{-2}: for an energy of 800 eV, the highest ion charge was equal to 6; for 1050 eV, it was equal to 8, and for the highest energy it was equal to 10 (Fig. 7). It is noteworthy that a self-bleaching effect was also discovered for an energy of 2000 eV.

4. Observations of hollow-ion spectra in laser plasmas

4.1 KK hollow ions

Hollow ions with two vacancies in the K shell (KK hollow ions) are the most remarkable representatives of hollow ions. For the first time, the emission spectrum of a KK hollow ion was presumably observed at the Nike laser facility [41] with a nanosecond pulse duration; its interpretation in terms of the hollow-ion spectrum was proposed somewhat later [24]. Then, a spectrum of this type for multiply charged silicon ions produced in the target heating by a high-contrast subpicosecond pulse was recorded in Ref. [23] and interpreted as the spectrum of hollow ions. Model calculations carried out in Ref. [24] strongly supported this identification. For magnesium ions, spectra of this type were obtained and identified in Ref. [66]. There are several other papers (see, for instance, Refs [84, 85]), which reported observations of hollow-ion spectra, but no in-depth spectroscopic studies were carried out. Below we consider the results of the most detailed investigations of KK hollow-ion spectra [23–25, 66, 86].

4.1.1 Multiply charged hollow silicon ions in subpicosecond laser plasmas. The spectrum plotted in Fig. 1c was obtained at the Trident laser facility at Los Alamos National Laboratory [23]. Laser pulses were 500 fs long, had an energy of 550 mJ, and produced a peak intensity of about $(0.5–1) \times 10^{19}$ W cm^{-2}. The power contrast ratio between the main pulse and the natural nanosecond-long prepulse was no less than $10^{10} - 10^{11}$. Use was made of solid silicon targets. X-ray plasma spectra were observed on a spectrograph with a spherically bent mica crystal. Crystals with radii of curvature

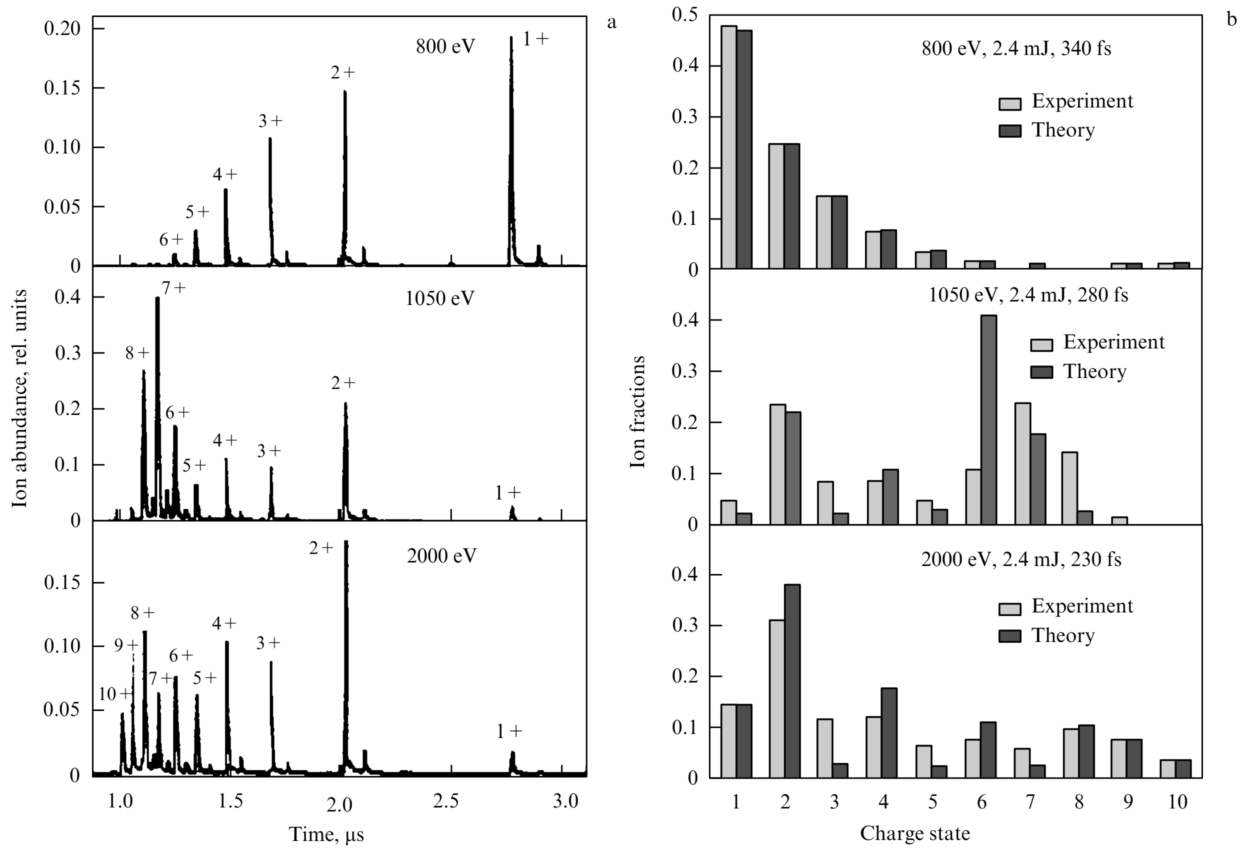

Figure 7. Ion abundance of different charge multiplicities in a neon target irradiated by LCLS laser pulses: (a) data of time-of-flight measurements, and (b) comparison with the simulations performed in Ref. [82].

of 100, 150, and 186 mm were utilized. The crystal, the plasma, and photographic film were arranged in FSSR-1D or FSSR-2D layouts, where FSSR-1D(2D) is a Focusing Spectrograph with one- or two-dimensional Spatial Resolution [6]. This enabled recording spectra simultaneously with high spectral ($\lambda/\delta\lambda = 10{,}000$) and spatial ($\delta x = 10$ μm) resolutions. The experimental setup is shown in Fig. 8. We emphasize that this setup is rather typical for spectroscopic studies of the laser plasmas of solid targets, and we shall refer to it in the subsequent consideration of other experiments.

Spectral structures in the 6.16–6.28-Å wavelength range (in the vicinity of the resonance line of Si XIV ions) may arise only from transitions from excited ion levels without 1s electrons. These transitions, as noted in Section 2.3, give rise to the emission of the resonance Ly_α line itself and its He-like dielectronic satellites, i.e. the lines whose upper energy levels are the doubly excited states of a two-electron ion. To find

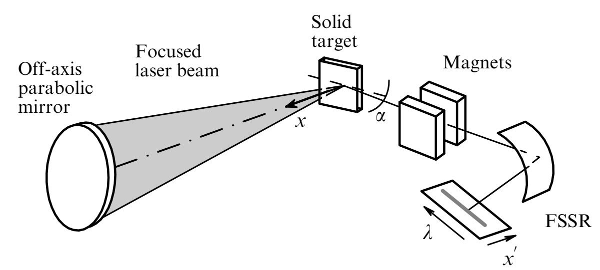

Figure 8. Schematic of the experiment to observe the spectra of hollow ions produced in the plasma of solid targets. The magnets protect the X-ray spectral instrument from fast charged particles.

additional spectral lines in the vicinity of the Ly_α line, atomic calculations were made using the Superstructure program [87]. Multiconfiguration wave functions of the bound states were constructed within the intermediate coupling approximation, with the inclusion of Breit–Pauli relativistic corrections. The autoionization matrix elements, which included continuum spectrum orbitals, were calculated within the distorted-wave approximation [88, 89].

These calculations suggest that the spectral range under investigation hosts a multitude of spectral lines arising from optical transitions in multielectron systems with the number of electrons $q \geqslant 3$ (Li-, Be-, ... like ions) with an empty K shell, i.e. from transitions in hollow ions. The state populations of the hollow ions with $q \geqslant 3$ in a coronal plasma are negligible, and the emission spectra of such a plasma arising from the ions with $q < 3$ have the characteristic form shown in Figs 1a and 1b. In an ultrahigh-density plasma with an electron density N_e exceeding the critical value N^* (for silicon plasmas, $N^* \sim 10^{22}$ cm^{-3}), the level population mechanisms nonlinear in N_e are responsible for a significant increase in hollow-ion state populations, thereby raising the amplitudes of the corresponding spectral lines. Notice that the most important consequences of this effect consist in (i) the collisional mixing of different l subshells in electron configurations with a given principal quantum number n, and (ii) a rise in importance of the role of additional population mechanisms for the states with $q \geqslant 3$, like dielectronic capture from excited states and three-body recombination [52, 53].

Figures 9a–9e display the calculated emission spectra of hollow ions with $q = 2$, 3, arising from the states with the

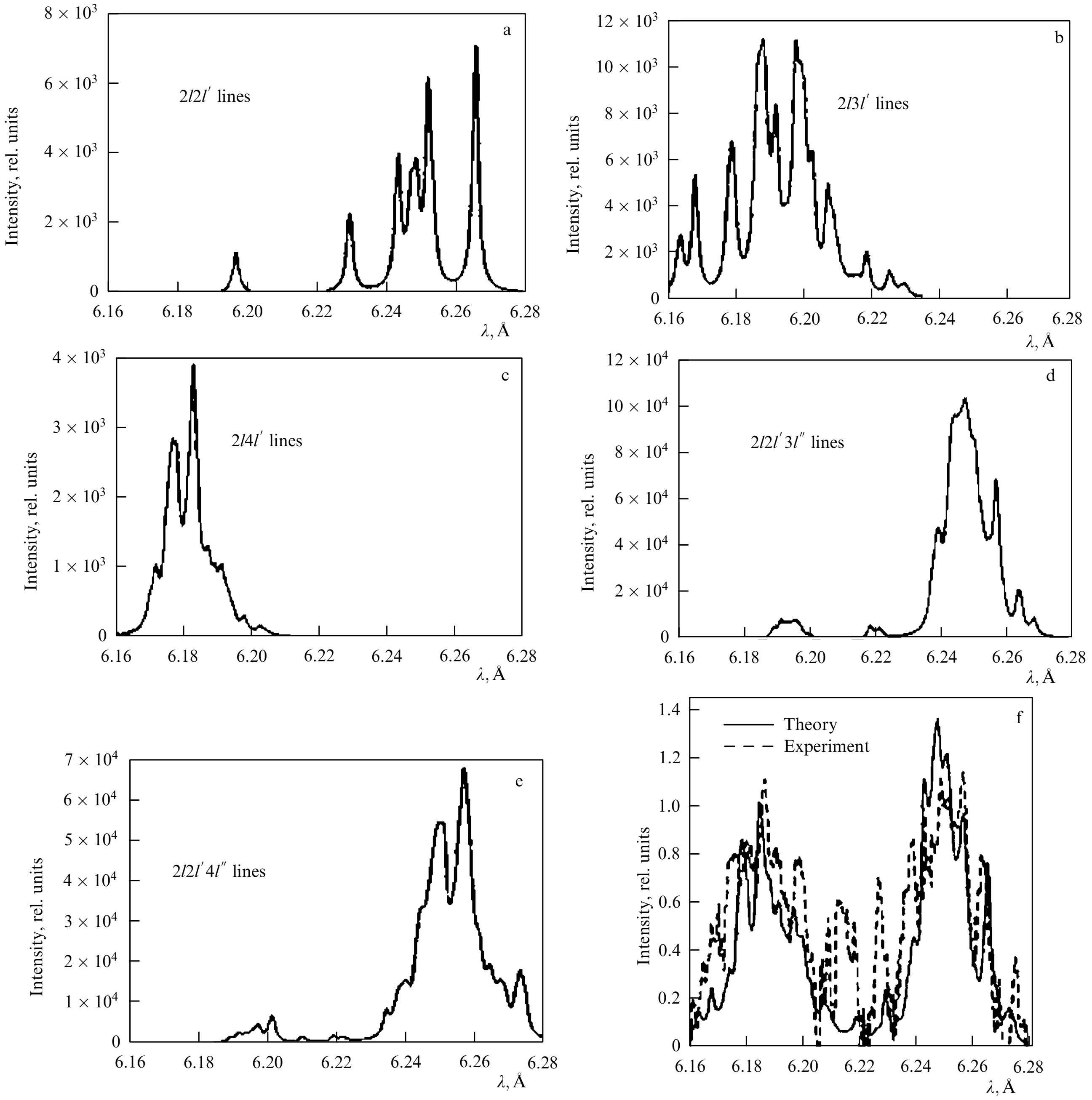

Figure 9. (a–e) Emission spectra of different hollow-ion states calculated for the Boltzmann population distribution over l subshells. (f) Comparison of the emission spectrum of a silicon femtosecond laser plasma with the simulated result for an LTE plasma with $T_e = 350$ eV and $N_e = 6 \times 10^{23}$ cm^{-3} [24].

following principal quantum number sets: $[2, n]$ and $[2, n, n_1]$. To construct the net emission spectrum requires, naturally, solving the corresponding system of kinetic equations. It is pertinent to note that the Boltzmann distribution over the l subshells allows the kinetic simulations to be substantially simplified due to a sharp decrease in the number of atomic levels under consideration. In this case, the kinetic system of equations should be solved not for individual atomic states, but for whole ion complexes characterized by different sets of principal quantum numbers. In an ultrahigh-density plasma, the ion distribution over various ion complexes is the Saha–Boltzmann distribution; the net spectrum corresponding to this case is plotted in Fig. 9f. It is noteworthy that the self-absorption of the Ly_α line was accounted for in the computation within the Biberman–Holstein approximation.

With reference to Fig. 9f, by and large the synthesized spectrum is in rather good agreement with experimental data. Its discordance with the observed spectra (the presence of two inexplicable peaks at about $\lambda = 6.215$ Å and $\lambda = 6.23$ Å and some underestimation of the observed intensity throughout the spectral domain) is due to the neglect of the hollow ion complexes of the form $[2, n, n]$ with $n \geqslant 3$ and $[2, n]$ with $n > 4$, as well as of electron configurations with $q \geqslant 4$.

The satisfactory agreement of experimental spectra with the results of model computations permitted a new type of quasicontinuous spectra produced by a high-contrast pulse in a subpicosecond laser plasma to be confidently ascribed to optical transitions in multiply charged hollow ions [24, 25]. Conclusions were also drawn in these papers that the laser plasma constitutes a natural source of hollow ions, which open up fresh possibilities for analyzing their properties. The presence of ion states with empty K shells in such a plasma is a consequence of its ultrahigh density, which leads to violation of coronal conditions. A new type of spectral diagnostics was also proposed, which involved construction of the plasma emission spectrum, not from individual spectral lines, but from whole spectral complexes characterized by different sets of principal quantum numbers $[n, n_1, n_2]$. The results of model calculations made assuming the Boltzmann equilibrium were in good quantitative agreement with the measured spectra, thereby confirming that the adequate kinetic model of ultrahigh-density plasma must be constructed with the inclusion of hollow-ion states.

4.1.2 X-ray spectra of Mg hollow ions emitted from the plasma produced by short-wavelength XeCl laser radiation. As discussed in Section 4.1.1, high plasma densities are required, first of all, to produce the spectra of hollow ions. However, ultrahigh-density plasmas may be obtained not only with the use of ultrahigh-contrast femtosecond laser pulses, but also employing short-wavelength nanosecond lasers. To verify the assumption about the presence of hollow-ion lines in the spectrum of the plasma produced using a short-wavelength nanosecond laser, special experiments were performed at the Hercules (High energy repetitive CUOS laser system) laser facility at the Laboratories of ENEA, Frascati, Italy [66].

To heat the plasma in experiment [66], use was made of an excimer XeCl laser [90] with a wavelength of 0.308 μm. The energy of a laser pulse was equal to 2 J for a duration of 12 ns. The laser operated with a repetition rate of 10 Hz. Its radiation was focused on a spot 70 μm in diameter on the surface of a solid magnesium target, so that the intensity of laser radiation was rather low ($\approx 4 \times 10^{12}$ W cm^{-2}). The X-ray radiation of the plasma was recorded employing an FSSR-2D spectrograph with a spherically bent mica crystal [6, 91], which had a spectral resolving power of no less than $\lambda/\delta\lambda \approx 5000$ for a one-dimensional spatial resolution of $\delta x \approx 30$ μm in the direction of plasma expansion [i.e. along the normal to the target (see Fig. 8)].

Figure 10a depicts the emission spectrum of magnesium plasma in the 8.2–9.3 Å wavelength range recorded in Ref. [66]. Shown for comparison in Fig. 10b is the spectrum of magnesium plasma heated by an Nd laser with a pulse duration of 1 ns at an intensity of 10^{14} W cm^{-2}, which was previously obtained for the same wavelength range in Ref. [3]. It is noteworthy that spectra similar to those depicted in Fig. 10b had been previously observed not only in laser plasmas, but also in the plasma of exploding wires, pinches, and the solar corona (see, for instance, references in review [3]). Hereinafter, spectra of this form will be referred to as 'ordinary'. One can see from Fig. 10b that the ordinary emission spectra of magnesium plasma in the 8.2–9.3 Å wavelength range contain the resonance and intercombination lines of He-like Mg XI ion (the $\mathrm{He}_{\alpha 1}$ and $\mathrm{He}_{\alpha 2}$ lines), the resonance line of H-like Mg XII ions (the Ly_α line), and its dielectronic satellites which arise from the radiative decay of the autoionization states of He-like Mg XI ion (a group of lines in the 8.44–8.56 Å wavelength domain). With reference to Fig. 10, the main difference of the spectrum plotted in Fig. 10a from the ordinary one is in the emergence of additional quasicontinuous structures located in the 8.4–8.65 Å, 8.67–8.92 Å, and 8.94–9.15 Å wavelength regions.

In Section 2.3 we made already an attempt, proceeding from simple estimates, to conclude what spectral transitions

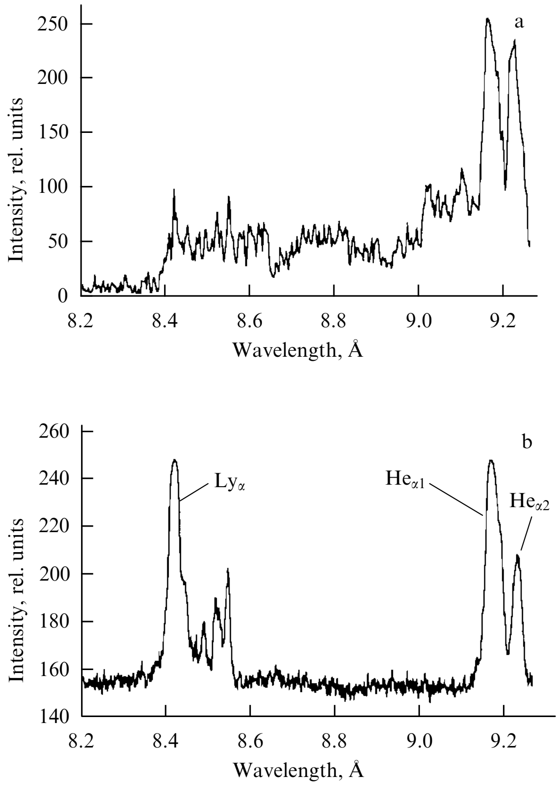

Figure 10. Emission in the 8.4–9.3 Å wavelength range from magnesium plasma heated by (a) a XeCl laser, and (b) an Nd laser [66].

may fall into the range between the Ly_α line of Mg XII ions and the He_α line of Mg XI ions. These estimates are borne out by the numerical calculations of the atomic structure of magnesium ions performed in Ref. [66]. For a preliminary estimate of the transition intensities and line positions of different spectral transitions, advantage was taken of the Cowan ATomic Structure (CATS) program, which enables calculating the emission properties of ions with different charge multiplicities within the average atomic configuration model [92]. Account was taken of all possible electron configurations for ions, ranging from Mg I to Mg XII, constructed from the orbitals 1s, 2s, 2p, 3s, 3p, and 3d. The emission spectra were calculated in the approximation of local thermodynamic equilibrium (LTE). The results are given in Fig. 11 for two values of the electron plasma temperature. We emphasize that the ground state populations of ions with different charge multiplicities were assumed to be equal in these calculations, i.e. the ionization balance was not calculated.

Figure 11a demonstrates the results of calculations for a relatively low temperature of 100 eV. In this case, the emission spectrum constructed assuming LTE is dominated by satellite structures, since the hollow-ion state populations are very low. As the temperature increases, the situation changes, and optical transitions in hollow ions begin to prevail (see Fig. 11b, constructed for $T_e = 1000$ eV). As can be seen from Fig. 11, for each degree of ionization the emission spectrum consists of several rather broad peaks, which differ by combinations of occupation numbers with conservation of their sum.

The most significant difference between Figs 11a and 11b consists in the fact that the optical transitions in KK hollow ions are confined to the $\lambda > 8.4$ Å region, and the observed

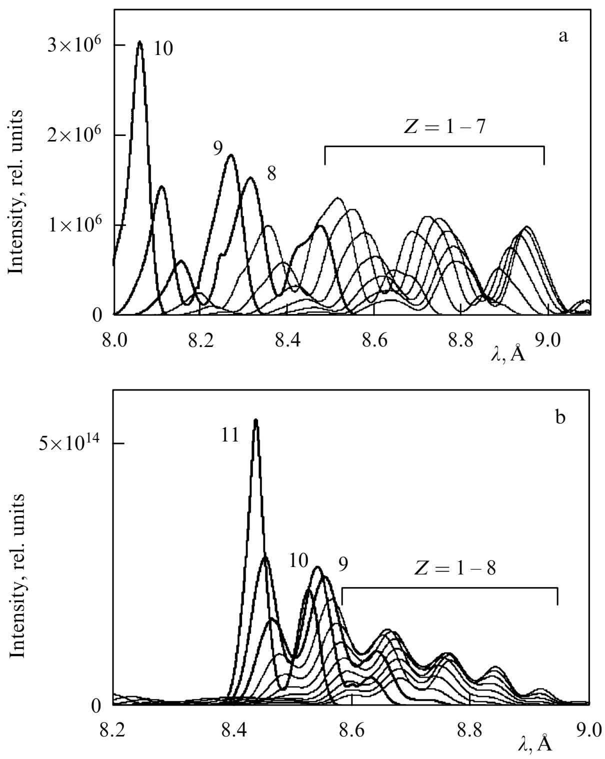

Figure 11. (a) Emission spectrum of the $n' = 3 - n = 1$ transitions in magnesium ions calculated within the average atomic configuration approximation. (b) Emission spectrum of the $n' = 2 - n = 1$ transitions in hollow magnesium ions. The numbers alongside the curves stand for the spectroscopic symbol of an ion [66].

spectrum should have a sharp edge at this wavelength, when these transitions are prevalent. When the satellites and KL hollow ions are prevalent, this sharp edge does not manifest itself, and the spectral peaks are rather uniformly distributed over the wavelength range between 8 and 9 Å (Fig. 11a). Since the observed spectra clearly exhibit a sharp edge in the vicinity of $\lambda = 8.4$ Å (see Fig. 10), this alone suggests that the observed structures are attributable to the optical transitions in multiply charged hollow magnesium ions. There is an additional indication that the observed features of the spectrum are associated with precisely the radiative transitions in hollow ions, rather than with satellite structures of low-ionized ions. As noted in Section 3, the excitation of such structures in a cool plasma requires the presence of a fast electron beam giving rise to the generation of fast ions, i.e. ions with energies significantly higher than the thermal one. Our earlier X-ray spectroscopic studies showed that the plasma production at the Hercules facility is not accompanied by fast ion generation, so the presence of a fast electron beam is therefore unlikely.

The average atomic configuration model employed in constructing the intensity curves in Fig. 11 allows nothing more than an estimate of the position of the center of gravity of the envelope for a group of lines emitted in the radiative decay of one configuration or another, but not its shape. That is why, detailed calculations of the atomic characteristics of isolated ions were performed in Ref. [66] with the aid of computational programs which enabled determining the wavelength and the probability of every individual spectral transition from the set under consideration. The wavelength region 8.4–8.7 Å, which contained, as is evident from Fig. 11b, the transitions of the hollow ions with greatest charge multiplicities, was investigated at greatest length. It is noteworthy that the least excited atomic configurations in plasmas are, as a rule, the most populated ones. The only exceptions to this general rule are a dense recombining plasma in which the recombination flux goes through highly excited configurations, thereby leading to their efficient population, and a plasma in which resonance processes occur (charge exchange, photoexcitation, or photoionization by external narrow-band radiation), which are responsible for the selective population of certain configurations. That is why, of all possible electron configurations, the paper [66] considered the least excited configurations with lowest occupation numbers n_i; specifically, the paper [66] restricted themselves to the following sets of occupation numbers:

(1) for He-like ions ($\sum n_i = 2$): $n_2 = 2$; $n_2 = 1$, $n_3 = 1$; $n_2 = 1, n_4 = 1$;

(2) for Li-like ions ($\sum n_i = 3$): $n_2 = 3$; $n_2 = 2$, $n_3 = 1$; $n_2 = 2$, $n_4 = 1$; $n_2 = 2$, $n_5 = 1$; $n_2 = 1$, $n_3 = 2$; $n_2 = 1$, $n_3 = 1, n_4 = 1$;

(3) for Be-like ions ($\sum n_i = 4$): $n_2 = 4$; $n_2 = 3$, $n_3 = 1$; $n_2 = 3, n_4 = 1$; $n_2 = 3, n_5 = 1$; $n_2 = 2, n_3 = 2$; $n_2 = 2, n_3 = 1$, $n_4 = 1$; $n_2 = 1, n_3 = 3$;

(4) for B-like ions ($\sum n_i = 5$): $n_2 = 5$; $n_2 = 4$, $n_3 = 1$; $n_2 = 3, n_4 = 2$; $n_2 = 2, n_5 = 3$; $n_2 = 1, n_3 = 4$.

The wavelengths and oscillator strengths of all transitions from the above configurations were calculated within the intermediate coupling approximation with the inclusion of configuration interaction.

For each set of occupation numbers there is a huge number (up to several thousand) of closely located lines, which make up the so-called unresolved transition array (UTA). (Exceptions are provided by only two electron configurations, for which the number of lines is not high; they form several well-resolved spectral peaks.) When the plasma density is not too low (in the case of experiments under consideration, the plasma density near the target amounted to 10^{22} cm^{-3}), local thermodynamic equilibrium is realized within the levels for one configuration, and the emission plasma spectrum associated with this configuration is described by the following sum

$$S(\lambda, n_1, n_2, n_3, \ldots) = \sum_{i,k} g_i A_{ik} f(\lambda - \lambda_{ik}) \exp\left(-\frac{E_i}{k_B T_e}\right), \quad (2)$$

where g_i and E_i are the statistical weight of a level and its energy, A_{ik} is the radiative transition probability, and $f(\lambda - \lambda_{ik})$ is the spectral shape of a transition. Sum (2), which is taken over all levels of a given configuration, is the spectral function of this configuration. The net emission $S(\lambda)$ of an optically thin plasma is defined by the expression

$$S(\lambda) = \sum_{n_1, n_2, \ldots} \frac{S(\lambda, n_1, n_2, \ldots)\, N(n_1, n_2, \ldots)}{g(n_1, n_2, \ldots)}, \quad (3)$$

where $N(n_1, n_2, \ldots)$ and $g(n_1, n_2, \ldots)$ are the population and statistical weight of the corresponding configuration.

Sum (2) is conveniently divided into parts corresponding to configurations with a fixed total number of electrons $M = \sum_i n_i$. If it is assumed that LTE is also realized for all isoelectronic configurations, it is possible to calculate the net spectral function of each ion. These functions will depend on the plasma temperature (which determines the relative populations of different isoelectronic configurations) and the intrinsic spectral shape $f(\lambda - \lambda_{ik})$ of the transition. These spectral functions calculated for two-, three-, four-, and five-electron ions assuming Gaussian profiles 0.004 Å in width are plotted in Fig. 12, which clearly demonstrates the following general features:

• For each isoelectronic sequence, the transitions in hollow ions are confined in the wavelength range from $\lambda(\mathrm{Ly}_\alpha)$ to some quantity $\lambda_{\max}(M)$, which depends on the number of electrons M in the ion.

• The quantity $\lambda_{\max}(M)$ is an increasing function of M.

• For a low temperature, the spectral functions are concentrated near the $\lambda_{\max}(M)$ wavelength; as the temperature increases, they spread over the entire region from $\lambda(\mathrm{Ly}_\alpha)$ to $\lambda_{\max}(M)$.

This behavior of the spectral functions is qualitatively quite explicable. For a low temperature, only the least excited configurations of hollow ions of the $(2l)^M$ type are rather densely populated. For these configurations, the wavelength shift is largest and increases with increasing M, as discussed above. As the temperature increases, the higher excited $(2l)^{n_2}(3l)^{n_3}\ldots$ type configurations, for which the screening effect is weaker, come to play a progressively more important part, and the spectral functions begin to shift to the shorter-wavelength side.

It would be instructive to compare the relative position of the spectral functions of ions with different numbers of electrons. From Fig. 13, in which such a comparison is made for $T_e = 100$ eV, it is evident that the spectral functions of different ions overlap, despite a systematic shift towards longer wavelengths with increasing M. Notice that narrow peaks in the spectral functions are formed, as a rule, not due to a single or several strong transitions, but due to an accidental coincidence of the wavelengths of a very large number of spectral lines.

A high degree of accuracy can hardly be expected from calculations of the atomic characteristics of complex atomic systems with a large number of open shells, and therefore the true spectral functions most likely will not have such clearly defined peaks and will more uniformly fill the corresponding spectral range. Unfortunately, to date it is impossible to make an *a priori* estimate of the accuracy of wavelength calculations for transitions in hollow ions with three or more electrons.

One can see from Fig. 12 that the spectral functions corresponding to different electron configurations are of the same order of magnitude at their maxima. This has the following implication: when the concentrations of the plasma ions of different isoelectronic sequences do not differ greatly (i.e. are of the same order of magnitude), all the configurations considered above will make an appreciable contribution to the net plasma emission spectrum, and this spectrum will be inherently complex and quasicontinuous.

For instance, shown in Fig. 13 is the spectrum calculated for $T_e = 100$ eV and the following $(2l)^{n_2}$ configuration population ratios: $N[(2l)^2]/g[(2l)^2] : N[(2l)^3]/g[(2l)^3] : N[(2l)^4]/g[(2l)^4] : N[(2l)^5]/g[(2l)^5] = 4:1:1:1$. One can

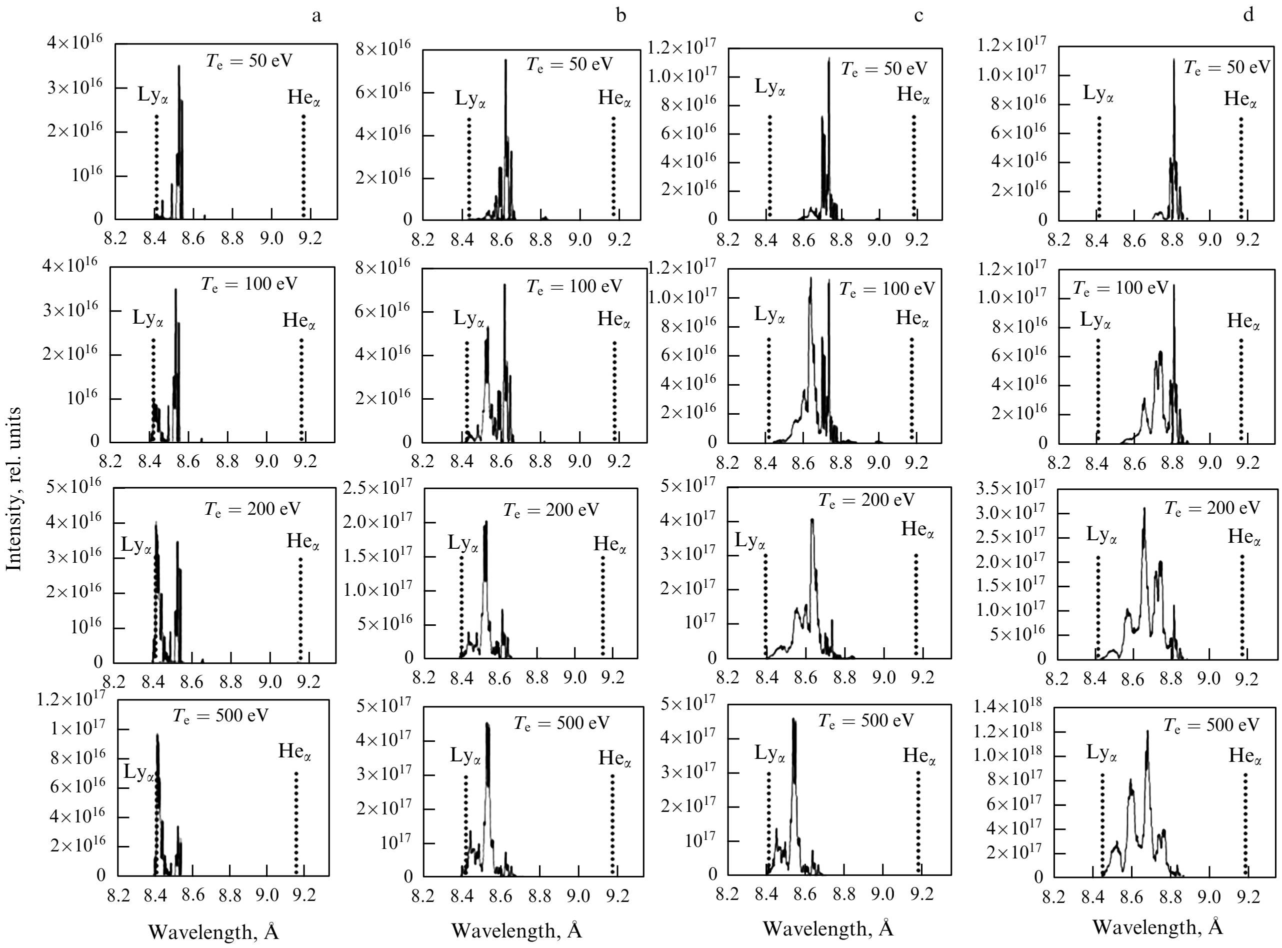

Figure 12. Spectral functions of Mg XI (a), Mg X (b), Mg IX (c), and Mg VIII (d) ions calculated in the LTE approximation for different plasma temperatures [66].

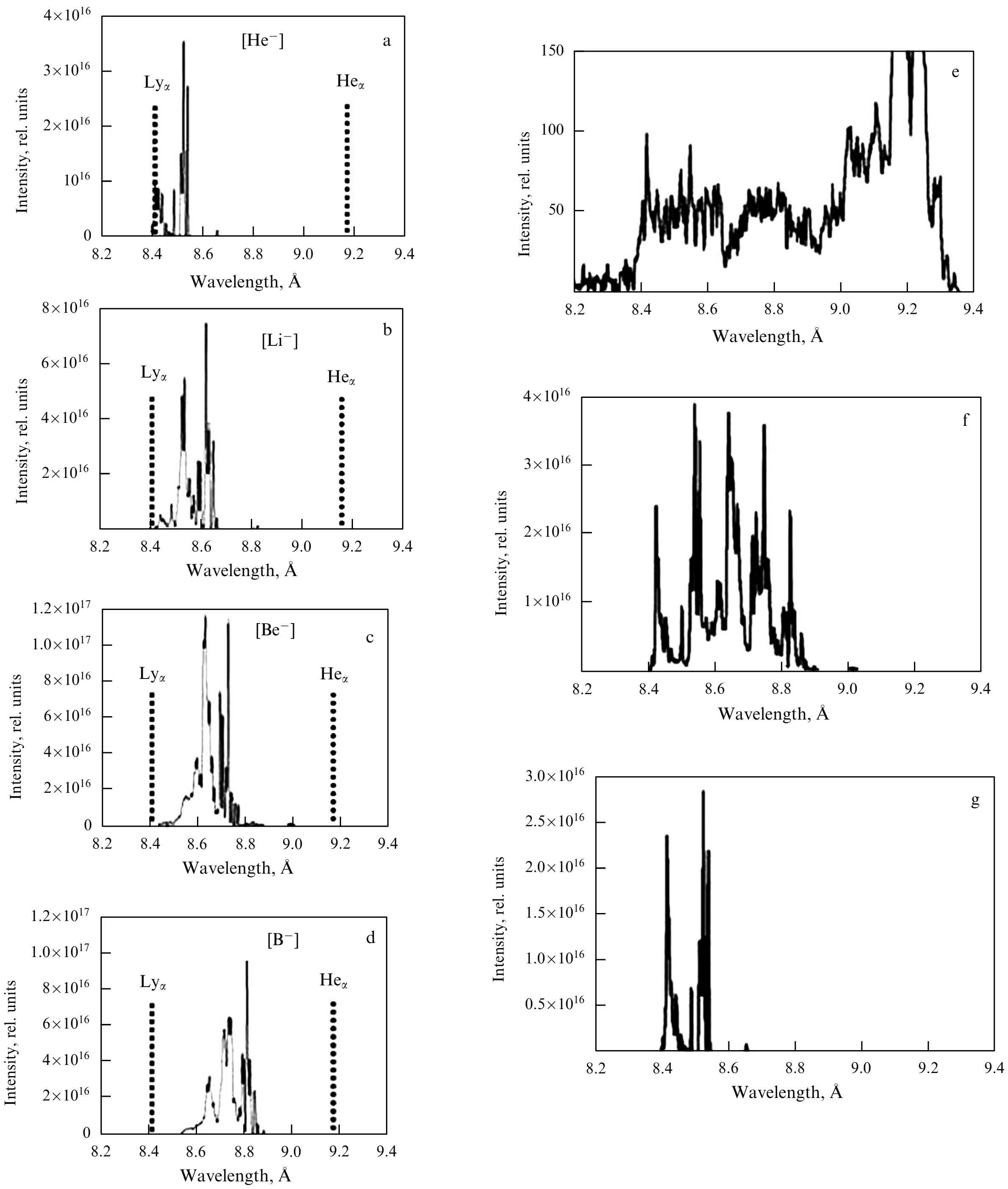

Figure 13. (a–d) Spectral functions of magnesium ions of different isoelectronic sequences for $T_e = 100$ eV. Radiation of magnesium plasma in the 8.4–9.3 Å range: (e) observation in plasma heated by an excimer laser; (f) theoretical model, which includes transitions in hollow ions with the number of electrons $M < 6$, and (g) inclusion of only dielectronic satellites [66].

see from the figure that the ion configurations with 2–5 electrons considered above form an unresolved transition array in the 8.4–8.8 Å wavelength domain. Also plotted in Fig. 13 are the experimental spectrum obtained by the authors of the present review in Ref. [66] and the emission spectrum calculated with the inclusion of only the dielectronic satellites of the Mg XII ion Ly_α line.

The following conclusions can be drawn on comparing these three spectra.

(1) The dielectronic satellites of the Ly_α line cannot provide even a qualitative explanation for the emission spectrum of the plasma produced by the short-wavelength nanosecond excimer laser, although they nicely explain the previously observed spectra of plasma heated by infrared lasers of nano- and picosecond durations.

(2) Radiative transitions in hollow magnesium ions with 3–5 electrons produce a quasicontinuous spectrum which both spans the spectral region between the Ly_α line and its dielectronic satellites and extends beyond its long-wavelength edge.

(3) The emission spectrum in the 8.4–8.7 Å range is formed due both to dielectronic satellites and to transitions in hollow Li-, Be-, and B-like magnesium ions.

(4) The spectrum in the region $\lambda > 8.7$ Å may be formed only due to radiative transitions in hollow ions with the number of electrons $M \geqslant 4$.

Naturally, the model spectrum depicted in Fig. 13 cannot pretend to a quantitative description of the observed spectrum throughout the 8.4–9.2 Å range for several reasons, the main ones of which are as follows.

First, we considered here only ions with the number of electrons $M < 6$. The undiscussed transitions in hollow C-, N-, and O-like ions should, on the one hand, form the emission spectrum in the $\lambda = 8.7-9.2$ Å range and, on the other hand, make a contribution (though a moderate one) to the shorter wavelength 8.4–8.7 Å range.

Second, as discussed above, the calculated spectral functions of multielectron configurations contain uncertainties (related primarily to the positions of individual spectral transitions), which may substantially change their shape.

Third, the experimental spectrum represents the luminosity of plasma averaged over its lifetime. In the course of plasma evolution, its parameters (density, temperature, and ion composition) vary strongly. Meanwhile, as is clear from Figs 12c, 12d, and 13, even a variation of only the temperature has a very strong effect on the spectral functions associated with a given ion. Averaging the spectral functions over the temperature yields a fuzzier spectrum structure with less clearly defined peaks, which, strictly speaking, shows up in the experimental spectrum.

Therefore, it was shown in paper [66] that the recorded spectral structures arose from radiative transitions in KK hollow ions, which had previously been observed in laser plasmas only at femtosecond and picosecond ultrahigh-power laser facilities for very high-contrast laser pulses, and for low-charged ions in the interaction of high-intensity relativistic ion beams with solids. As noted in Ref. [66], elucidating the hollow-ion production mechanisms in laser plasma calls for both systematic experimental X-ray spectroscopic studies and detailed calculations of collisional-radiative ion kinetics in inhomogeneous nonstationary plasmas with the inclusion of possible processes of photoionization by intrinsic plasma radiation and ion charge exchange.

We notice once again that the spectral range between the satellites of the resonance line of H-like ions and the resonance line of He-like ions, where the spectra of hollow ion configurations are not blended by other transitions, is best suited for experimental exploration. Until recently it was assumed that this range did not contain any spectral transitions whatsoever, and so no systematic investigations into the laser plasma radiation were carried out there. We emphasize once again that these investigations, as shown in Ref. [66], do not necessarily call for the employment of expensive ultrahigh-power high-contrast femtosecond laser facilities or accelerator facilities; instead, use can be made of relatively simple plasma sources based on a nanosecond pulsed short-wavelength laser with a moderate output power.

One can see that the model spectrum depicted in Fig. 13f provides a good description of the experimental spectrum in the 8.4–8.8 Å wavelength range; however, unlike the experimental spectrum, it does not give any lines in the longer-wavelength region. More recently, papers [93–95] reported that this was due to the fact that the previously performed modeling neglected several possible electron configurations in KK and KL hollow ions.

The new calculations performed in Refs [93–95] were based on the ATOMIC program within the mixed unresolved transition array (MUTA) approximation. This made it possible to add several significant configurations in the calculation and, in so doing, retain the computation time at an acceptable level. With reference to Fig. 14, the data of the new calculations bore out the assumption that the observed spectrum was formed by radiative transitions in hollow ions and allowed a virtually complete description of the spectrum observed.

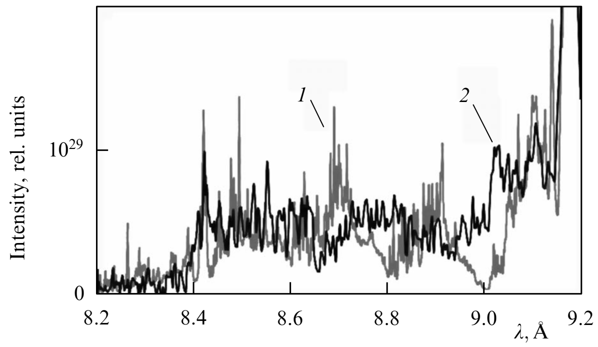

Figure 14. Spectrum of Mg plasma (*1*) calculated using the ATOMIC program with the inclusion of hollow ions [93], and experimental spectrum (*2*) [66].

4.1.3 Role of charge exchange in the formation of KK hollow nitrogen ions in the interaction of femtosecond laser pulses with a high-pressure gas. When a gas is utilized as a laser target, there are favorable conditions for the penetration of multiply charged ions, which are generated in the focal region, into peripheral regions containing primarily low-charged ions and even neutral atoms of the gas. This has the consequence that the charge exchange processes mentioned in Section 3 may give rise to an efficient population of the states of hollow ions. This effect was first discovered and explained in paper [86], which was dedicated to the experimental and theoretical investigation of intense femtosecond laser pulses with high-pressure nitrogen.

The experiments of Ref. [86] were performed on the titanium-sapphire laser of the Saclay Research Center (France). Laser pulses with a linear p-polarization were focused onto a pulsed gas target. The jet of nitrogen had a transverse dimension of about 20 mm, with strong density gradients at its boundaries. The atomic number density was amounted to 1.5×10^{19} cm^{-3} for the highest pressure in the valve equal to 20 bar. The pulse energy was 750 mJ, the wavelength was 790 nm, and the laser contrast ratio was 10^5. A laser beam 80 mm in diameter was focused with an off-axis parabolic mirror with an aperture ratio of 1/2.35, and the radius of the focal spot was equal to 8 μm. The corresponding Rayleigh length and intensity were equal to 70 μm and 10^{19} W cm^{-2}. Under this intensity, the optical field ionization could take place up to the instant of formation of bare nitrogen nuclei [96]. Figure 15 depicts the experimental setup typical for spectroscopic investigations of the plasma of pulsed gas or cluster targets.

The space-resolved X-ray spectra of nitrogen ions were recorded using a spectrograph with a spherical mica crystal [6, 97] bent to a radius of 150 mm, which was located at a distance of 250 mm from the plasma. The average Bragg angle was equal to approximately 75°. The spectral resolving power was no less than 2000, and the spatial resolution was

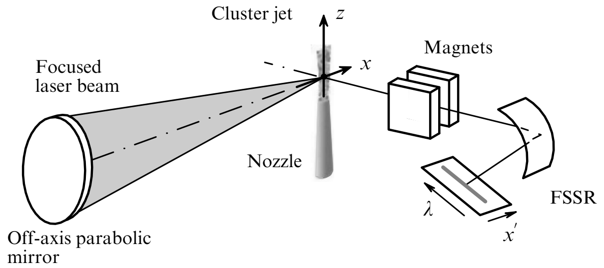

Figure 15. Schematics of the experiment for observing the spectra of hollow ions produced in the plasma of gas or cluster targets. The magnets protect the X-ray spectral instrument from fast charged particles.

$\delta x = 30$ μm in the direction of propagation of the laser radiation.

Figure 16a displays two experimental nitrogen emission spectra recorded for different gas pressures in the 1.88–1.96 nm wavelength range. One can see very broad structures about the resonance lines of the H-like ion. However, calculations taking into account the quasistatic ion field, broadening due to collisions with electrons, and Doppler broadening suggest that experimental line widths are far broader than the theoretical ones for the highest possible electron density (2×10^{20} cm^{-3}) (the theoretical spectrum is exemplified in Fig. 16b). A good correlation between separate peaks in different experimental spectra (Fig. 16a) suggests that they are not noise and represent some spectral structures. The authors of Ref. [86] hypothesized that these structures arise from transitions from radiative the highly excited $nln'l'$ states of hollow He-like nitrogen ions.

Atomic calculations performed using the multiconfiguration Hartree–Fock method with the inclusion of relativistic corrections for hollow configurations $3l5l'$, $4l5l'$, $5l5l'$, $3l6l'$, $4l6l'$, $5l6l'$, $6l6l'$, $3l7l'$, $4l7l'$, $5l7l'$, $6l7l'$, $7l7l'$, $3l8l'$, $4l8l'$, $5l8l'$, $6l8l'$, $7l8l'$, and $8l8l'$ confirmed this assumption, at least for the wavelengths of the observed spectral peaks. It turned out that the spectra of the structures listed above are really quite broad because of the mutual overlap of a huge number of closely spaced transitions and lie in the spectral region of interest. Furthermore, the total emission spectrum of these hollow ion states provides a qualitatively and even quantitatively good description of the experimental spectrum (a comparison is given in Fig. 16c), with the exception of the H-like ion resonance lines themselves. This signifies that, in this case, the hollow ion states for some reasons are anomalously densely populated in comparison with the singly excited states of hydrogen-like ions. To explain this anomalous behavior of level populations, the authors of Ref. [86] proposed a physical mechanism involving charge exchange in collisions of multiply charged and low-charged nitrogen ions. The scenario of this mechanism is as follows.

After the optical field ionization of N_2 molecules to the state of bare nuclei, they penetrate the surrounding gas which contains neutral atoms or singly and doubly ionized ions (Fig. 17). The reason is that the laser intensity decreases rapidly with distance from the central spot, and at distances of

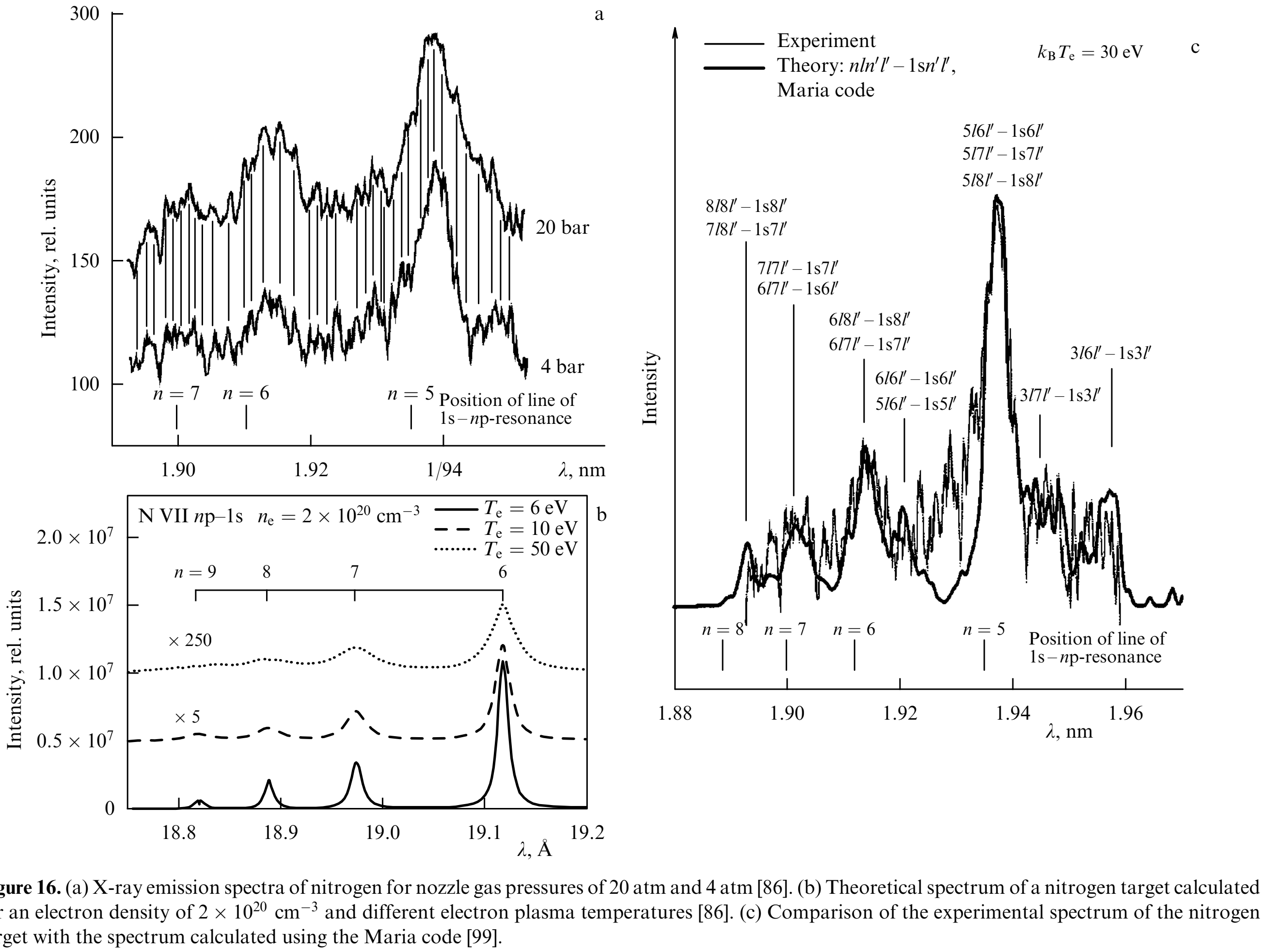

Figure 16. (a) X-ray emission spectra of nitrogen for nozzle gas pressures of 20 atm and 4 atm [86]. (b) Theoretical spectrum of a nitrogen target calculated for an electron density of 2×10^{20} cm^{-3} and different electron plasma temperatures [86]. (c) Comparison of the experimental spectrum of the nitrogen target with the spectrum calculated using the Maria code [99].

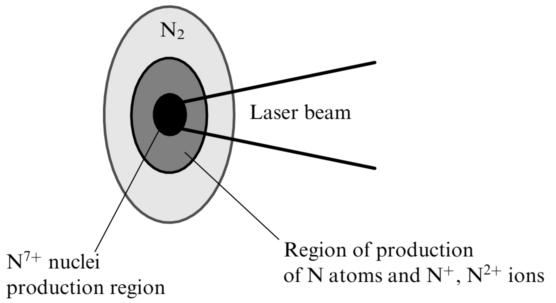

Figure 17. Production of ions of different charge multiplicities in different spatial regions of a gas target.

about 30 μm the laser field cannot ionize even N_2 molecules. We note, however, that N_2 molecules, even though far away from the central spot, may be destroyed by sufficiently high-energy particles (photons and electrons) generated in the central region. That is why, in accordance with Ref. [86], it will be assumed that the nuclei collide with N^0, N^+, and N^{2+} ions, resulting in the following single- or double-electron charge-exchange reactions:

$$N^{6+} + N^0 \to N^{5+}(nl) + N^{1+}, N^{6+} + N^{1+} \to N^{5+}(nl) + N^{2+}, N^{6+} + N^{2+} \to N^{5+}(nl) + N^{3+}, \quad (4)$$

$$N^{6+} + N^0 \to N^{4+}(nln'l') + N^{2+}, N^{6+} + N^{1+} \to N^{4+}(nln'l') + N^{3+}, N^{6+} + N^{2+} \to N^{4+}(nln'l') + N^{4+}. \quad (5)$$

In the low-velocity limit $\{v < 2.18 \times 10^8 (I/\mathrm{Ry})^{1/2}\ [\mathrm{cm\ s^{-1}}]\}$, the corresponding cross sections may be estimated using the classical above-barrier model [98]:

$$\sigma_1 = \pi a_0^2 (R_1^2 - R_2^2)\,, \quad \sigma_2 = \pi a_0^2 R_2^2\,,$$

where $R_1 = 2\mathrm{Ry}(2Z^{1/2} + 1)/I_1$, $R_2 = 2\mathrm{Ry}[2(Z-1)^{1/2} + 1]/I_2$, $a_0 = 5.29 \times 10^{-9}$ cm is the Bohr radius, Ry is the Rydberg energy, $\mathrm{Ry} = e^2/(2a_0) = 13.61$ eV, and I_1 and I_2 are the ionization potentials in electron-volts.

For the charge exchange with nitrogen molecules, one has $I_1 = I(N_2 \to N_2^{1+}) = 15.3$ eV and $I_2 = I(N_2 \to 2N^{1+}) = 23.5$ eV, and the cross sections are $\sigma_1 = 6 \times 10^{-15}$ cm^2, $\sigma_2 = 4 \times 10^{-15}$ cm^2. For the charge exchange with the first ion, it appears that $I_1 = 29.6$ eV, $I_2 = 47.4$ eV, and $\sigma_1 = 2 \times 10^{-15}$ cm^2, $\sigma_2 = 1 \times 10^{-15}$ cm^2. By assuming that the peripheral region temperature equals ~ 10 eV (in this case, the N^{1+} ion fraction amounts to about 10%), it is possible to estimate the probabilities of level population by charge exchange processes, i.e. the quantities $n(N^{1+})\,v\sigma_1 = 2 \times 10^{11}$ s^{-1}, $n(N^{1+})\,v\sigma_2 = 1 \times 10^{11}$ s^{-1}, and compare them with the population probabilities due to recombination mechanisms, which turn out to be on the order of 10^{10} s^{-1} for three-body recombination, and on the order of 2×10^9 s^{-1} for radiative recombination [86]. Evidently, the charge exchange mechanisms do turn out to be most significant in the population of hollow ion states. In this case, according to the classical charge exchange theory, the charge exchange will populate primarily the states with principal quantum numbers defined by the expression [99]

$$n_{\mathrm{f}} = Z\left(\frac{\mathrm{Ry}}{I}\right)^{1/2} \frac{2Z^{1/2} + 1}{Z + 2Z^{1/2}}\,, \quad (6)$$

which yields $n_{\mathrm{f}} = 3$ and 4 for I_1 and I_2, respectively. In dense plasmas, however, the electron capture may also occur through highly excited states [100], since the charge exchange cross section increases rapidly with a decrease in ionization potential, and the populations of excited states in dense plasma are not too low. As is clear from formula (6), hollow-ion states with high n_{f} will be populated in this case. For instance, the values of n_{f} will lie in the range 5–8 in the charge exchange on the 2p3*l* and 2p4*l* states. These are precisely the n_{f} values which were accounted for in Ref. [86] in modeling the experimental spectrum depicted in Fig. 16c.

4.2 KL hollow ions

Investigations into the spectra of KL hollow ions are a much more intricate task than the case of KK hollow ions considered above. First, these spectra consist, as a rule, of a substantially greater number of closely located spectral transitions, because in this case the initial electron configuration of a transition involves a larger number of open electron shells. Second, the presence of an additional hole in the L shell (and not in the K shell) gives a significantly lower wavelength shift for these transitions, and they lie virtually in the same spectral region as ordinary dielectronic satellites. For instance, the hollow-ion spectra lying near the resonance lines of multiply charged Ne-like ions should overlap with Na-, Mg-, ... like satellites, and it is extremely difficult to single them out in the observed spectrum and, without performing reliable precise calculations of the atomic structures and detailed kinetic computations, is hardly possible at all. This is the reason why, although the significance of these transitions was first emphasized by Rhodes and his collaborators [84, 85, 101, 102], we cast doubt on the identification of xenon cluster emission spectra as the spectra of KL hollow ions proposed by the authors of these papers. More reliable are measurements for ions with not-too-large a total number of electrons, for instance, the data of Ref. [103] on the observation of KL hollow aluminium ions in a femtosecond laser plasma. In Sections 4.2.1–4.2.3 we consider the findings of Refs [103–106] in which the spectral features of the KL hollow ions were investigated in the greatest detail.

4.2.1 Observation of KL hollow ions in the emission spectra of aluminium plasma. To generate plasma in Ref. [103], advantage was taken of a femtosecond laser with a pulse duration of 80 fs, an energy of 2 mJ, and an intensity of $10^{16} - 10^{17}$ W cm^{-2} in the focal plane. The solid target had a layered structure: an aluminium layer was deposited onto a glass substrate, in one case a thin layer (about 20 nm), and in the other case a much thicker one (about 400 nm), with a 20-nm-thick titanium layer deposited above it. Following the authors of Ref. [103], the former target will be referred to as thin, and the latter one as thick. We emphasize that aluminium spectra in the thick-target case could be emitted only by dense plasma with a solid density, rather than the expanding high-temperature plasma corona.

As is evident from Fig. 18, which demonstrates the spectra recorded in Ref. [103], the X-ray spectrum changes radically with target type. Several satellite lines disappear in the case of the thick target; on the other hand, transitions appear in the KL hollow aluminium ions (denoted as KL in the figure) near the K_α line. Comparing their intensity with the K_α line intensity allows estimating the plasma electron temperature in the aluminium existence region. The best agreement

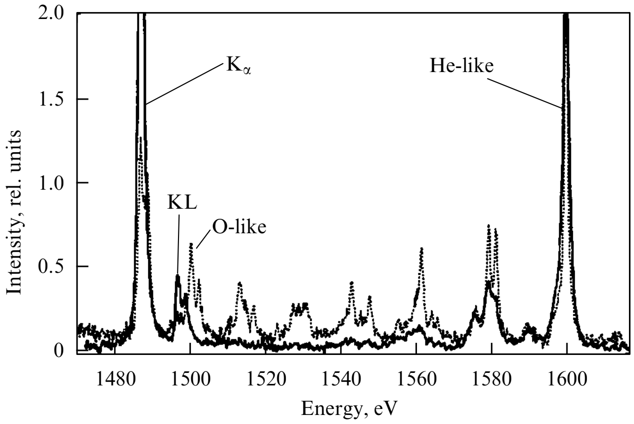

Figure 18. Aluminium spectra recorded in the interaction of a femtosecond laser pulse with structurally different targets at an intensity of 10^{16} W cm^{-2}: the dotted line stands for the thin target, and the solid line stands for the thick one [103].

between the experimental and theoretical spectra was revealed at $T_e = 20$ eV [103].

4.2.2 Role of KL hollow ions in the emission spectra of argon cluster plasmas. From the data given in Sections 4.1.1–4.1.3 and 4.2.1, it follows that hollow ions of different types may be produced using both solid-state and dense gas targets. Another modern class of targets, which shows good promise — not only for basic physical research, but also for important practical applications — comprises the so-called cluster targets (see, for instance, Refs [17, 69, 84, 85, 107–137]). In several recent papers it was revealed that the spectra of hollow ions are also present in the plasma radiation of cluster targets. First, we consider the results of investigations focusing on the interaction of femtosecond laser pulses with argon clusters.

In this section, we discuss experiments carried out at two laser facilities, which differ primarily by their laser contrast ratios.

The first experiments were performed using the titan: sapphire laser at the Kansai Photon Science Institute (KPSI), Kyoto, Japan. The experimental setup is schematized in Fig. 15. The pulse duration was equal to 30 fs for an energy of up to 360 mJ [72, 123, 138]. Two types of experiments were carried out. In one of them, a double Pockels cell was placed after the regenerative amplifier, which enabled attenuating the laser prepulse by about a factor of 5×10^4 relative to the main pulse. In the other case, two double Pockels cells were placed, and the laser prepulse was attenuated by a factor of $\approx 4.6 \times 10^6$. The laser radiation was focused with a gold-coated off-axis parabolic mirror with an aperture ratio of 1/3. The spot diameter at a level of $1/e^2$ was 11 μm, which was very close to the diffraction limit, and about 64% of the laser energy was concentrated on the focal spot. The energy of the laser pulses was varied between 49 and 115 mJ, and the pulse duration was varied over a very wide range from 30 fs to 1 ps. The intensity of laser radiation on the target ranged from 6×10^{16} to 2×10^{18} W cm^{-2}.

The argon cluster target was produced by letting argon with an initial pressure of 60 bar expand into a vacuum through a specially designed nozzle (three conic surfaces with different opening angles), which permitted obtaining clusters of a very large size, up to 1.5 μm [122, 138]. These large clusters were employed so as to prevent the laser prepulse from destroying them completely prior to the arrival of the main pulse, for the rate of cluster disintegration is determined primarily by the number of its constituent atoms [107]. The requisite cluster dimensions for laser prepulses with intensities in the range $10^{11} - 10^{14}$ W cm^{-2} had been earlier determined in experiments [120, 138].

Space-resolved X-ray plasma emission spectra were recorded using a spectrometer [97, 112, 133, 138, 139] with a spherically bent mica crystal ($R = 150$ mm) and an Andor DX420-BN X-ray CCD camera. The crystal, which was placed at a distance of 381.2 mm from the plasma source, was tuned to a central wavelength of 4.05 Å (a Bragg angle of 35.7° for the fourth-order reflection from the crystal). The detection range included the spectra of He-like argon and the corresponding satellite lines.

The observed spectrum was found to be strongly dependent on the amplitude of the laser prepulse; in this case, structures emerged in the wavelength region of about 4.14 and 4.17 Å at the lowest prepulse intensities, i.e. for the highest laser contrast, which were attributable to transitions in KL hollow ions. However, specially done atomic and kinetic calculations showed that these transitions were blended by dielectronic satellites, and their contribution to the observed spectrum intensity was not high enough to lay claim to their infallible identification.

Figure 19 displays an experimental spectrum obtained for the highest laser contrast and two theoretical spectra calculated with the inclusion and with neglect of radiative transitions in hollow ions. The model spectra correspond to an electron temperature of 50 eV, an atomic number density of 10^{22} cm^{-3}, and the presence of a 3% fraction of hot electrons with an electron temperature of 5 keV, with the values of plasma parameters selected from the best fit of the theoretical spectrum to the experimental one throughout the 3.9–4.2 Å wavelength range under investigation.

The main conclusions of paper [104] were as follows: first, the spectra of hollow ions (as is seen from Fig. 19) can make a contribution to the X-ray emission of cluster targets heated by femtosecond laser pulses and, second, to raise this contribution supposedly requires employing laser pulses with a much higher contrast. We suppose that raising

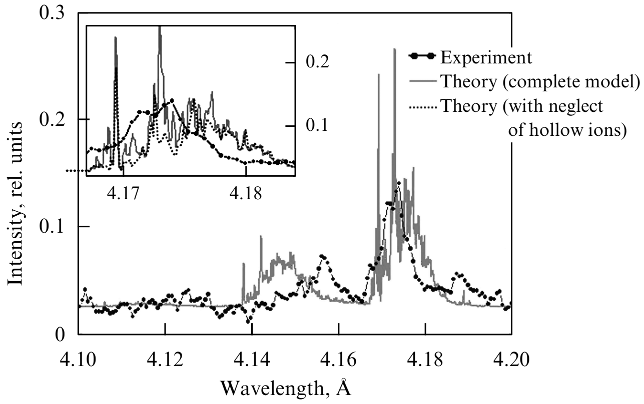

Figure 19. Comparison of the theoretical and experimental emission spectra of an argon cluster target. The calculation was made for $T_e = 50$ eV, an atomic number density of 2.5×10^5, and a 3% fraction of hot electrons with an energy of 5 keV. The dark curve fits experimental data, the grey curve stands for the complete calculation, and the dotted curve is the data calculated with neglect of hollow ions [104].

the contrast will substantially decrease the contribution to the observed spectrum from rarefied plasma regions produced by the prepulse, i.e. will allow observing the spectrum largely formed by only the most dense plasma regions. As we have repeatedly emphasized, it is in dense plasmas that favorable conditions emerge for hollow ion excitation. To verify this assumption, experiments were made with the JAEA-Kansai Advanced Relativistic ENgineering (J-KAREN) laser facility, KPSI, Japan [105].

In these experiments, the pulse duration was equal to 40 fs. The laser operated with a repetition rate of 1 Hz. The energy of a pulse focused on the cluster target amounted to 1 J, the focal spot diameter was 30 μm at a level of $1/e^2$. Therefore, the peak intensity amounted to 3.5×10^{18} W cm^{-2}. When use was made of an additional Pockels cell in combination with a saturable absorber, the laser contrast became very high, on the order of 10^{10}. The laser contrast could be lowered to 10^8 by switching off one of the Pockels cells and removing the saturable absorber, making it possible to study the sensitivity of the observed spectra to the contrast in the area of its extremely high values.

The target design was precisely the same as in the experiments described above. To record the spectrum, advantage was taken of the same spectrometer, but now it was tuned to a central wavelength of 3.88 Å (a 51.1° Bragg angle for the 4th order reflection from the mica crystal). This enabled observing the spectra between the Ly_α and K_α lines of argon in the 3.7–4.3 Å wavelength range with a spectral resolving power of 3000. Since mica crystals provide a good reflection in the 5th order as well, it was also possible to observe the spectra in the 3.0–3.5 Å wavelength range, which accommodate Rydberg transitions in He-like argon. The combination of the high-throughput spectrometer with a high-responsivity X-ray CCD enabled recording the spectra in one laser shot. Figure 20 exemplifies the typical spectra recorded for different laser pulse contrasts.

The spectral lines in both orders of reflection from the mica crystal are exhibited in Fig. 20. We note that primarily the $n \to 1$ transitions in He-like Ar XVII (n is the principal quantum number) for $n = 3$, 4, and 5 were observed in the 5th order (the lower wavelength scales). The high spectral resolution also allowed resolving with confidence the lines belonging to the hollow atoms of argon and the $\mathrm{K}_{\alpha 1,2}$ lines (Fig. 20b).

To correctly interpret the observed spectra, it is extremely important to invoke correct atomic and kinetic models. On the one hand, the model should include all degrees of ionization, since the observed spectrum contains the lines of all ions, beginning with the neutral atom and ending with the He-like Ar XVII ions. Furthermore, account must be taken of highly exotic configurations wherein one or more electrons are removed from the K and L shells of low-charged ions. On the other hand, the atomic states of each ion should be considered in sufficient detail with the inclusion of their splitting in all quantum numbers. All this calls for the treatment of a huge number of ion energy levels, which is fraught with major computational problems, despite the remarkable capabilities of modern computers. That is why the greatest possible simplification of the solvable atomic and kinetic problem is still a topical issue, even nowadays. In this connection, two types of calculations were performed in Ref. [68].

Calculations of the first type invoked the so-called MUTA model (for more details, see Refs [104, 105]), which treats the majority of spectral lines as an unresolved transition array, so that only the strongest spectral lines are individually traced. The number of states considered in this model is not too high (an advantage of the model), but very many separate atomic states are combined in some average configuration, which appreciably lowers, of course, the accuracy of their description (a disadvantage of the model). The atomic constants for MUTA-based modeling were calculated by a code package employed at the Los Alamos National Laboratory. The CATS code [92], which is a version of the well-known Cowan's code [140] adapted for running on supercomputers, was employed for calculating the wave functions, energy levels, oscillator strengths, and collision strengths (within the plane wave approximation). Electron impact ionization cross sections, photoionization cross sections, and autoionization rates were calculated using the General Ionization Processes in the Presence of Electrons and Radiation (GIPPER) code [141]. The three-body, radiative, and dielectronic recombination rates were determined according to the principle of detailed balance.

The following electron configurations were included in the MUTA model.

For all ions from neutral argon to Na-like argon, the calculations included the configurations $1s^2 2l^8 3l^w$,

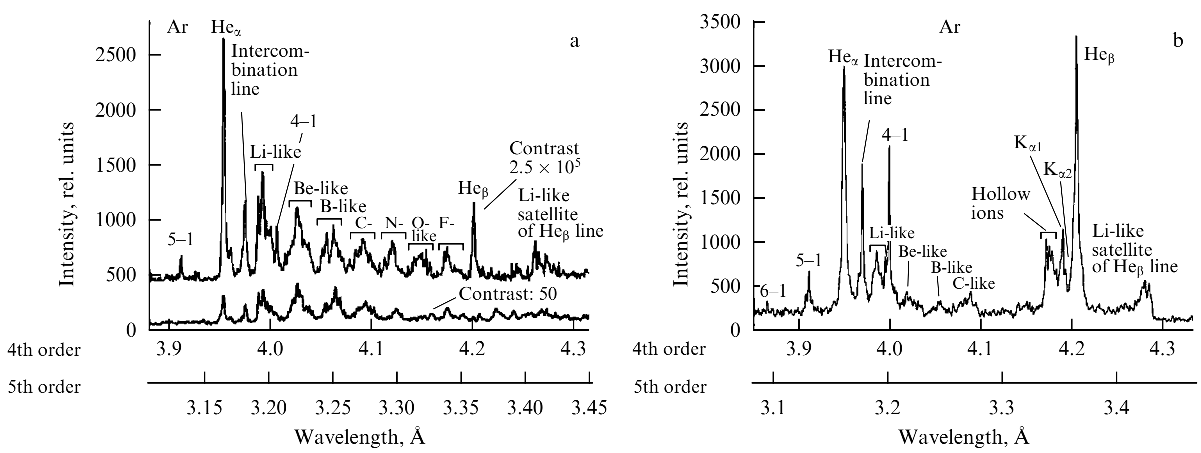

Figure 20. (a) Emission spectra of argon cluster plasmas for low, 50 (lower curve), and moderately high, 2.5×10^5 (upper curve), contrasts of laser pulses [109, 132]. Two wavelength scales correspond to the 4th and 5th orders of reflection from the crystal. (b) Emission spectra of the argon cluster plasma generated by an ultrahigh-contrast (10^{10}) laser pulse [105].

$1s^22l^83l^{w-1}4l'$, $1s^22l^83l^{w-1}5l'$, $1s^22l^73l^{w+1}$, $1s^22l^73l^w4l'$, $1s^22l^73l^w5l'$, $1s2l^83l^{w+1}$, $1s2l^83l^w4l'$, $1s2l^83l^w5l'$, $1s2l^73l^{w+2}$, $1s2l^73l^{w+1}4l'$, $1s2l^73l^{w+1}5l'$, $2l^83l^{w+2}$, $2l^83l^{w+1}4l'$, and $2l^83l^{w+1}5l'$. Simultaneously, it was assumed that $l' = 0-3$, and configurations with three or more electrons in the d shell were not considered. The value of w varied from 8 (for neutral argon) to 1 for Na-like argon ion.

For all ions beginning with the Ne-like argon and ending with the Li-like one, account was taken of the configurations $1s^22l^w$, $1s^22l^{w-1}3l'$, $1s^22l^{w-1}4l'$, $1s^22l^{w-1}5l'$, $1s2l^w3l'$, $1s2l^w4l'$, $1s2l^w5l'$, $1s2l^{w-1}(3l')^2$, $1s2l^{w-1}3l'4l''$, $1s2l^{w-1}3l'5l''$, $2l^w(3l')^2$, $2l^w3l'4l''$, and $2l^w3l'5l''$. In this case, also, l', $l'' = 0-3$, and w varied from 8 for Ne-like argon to 1 for the Li-like argon ion.

For He-like argon, account was taken of $1s^2$, $1snl\,(n=2-7)$, and $n'l'n''l''$ (n', $n'' = 2-5$) configurations, where $l = 0-6$ and $l'' = 0-3$. Included for H-like argon were all nl configurations with $l = 0-6$ and $n = 1-7$.

The MUTA model involved altogether 5600 electron configurations which described all argon ionization stages. The system of kinetic equations was solved using the ATOMIC program [142, 143] within the quasistationary approximation. In what follows, these calculations will be referred to as ATOMIC–MUTA computations.

Calculations of the second type were made with due regard for the fine structure of all the configurations under consideration. However, in this case account was taken only of C-like to H-like ions. Using this approach, naturally, the spectra arising from ions of highest multiplicities were described with a higher accuracy, but in doing so all ions from neutral argon to N-like argon, inclusively, were ignored. We note that, despite this limitation, the system of kinetic equations comprised 23,000 ion levels and its solution required computation times longer by several orders of magnitude. In what follows, these calculations will be referred to as ATOMIC–FS (fine structure) calculations.

Two series of experiments were also carried out. The first involved variations of laser contrast (Fig. 21a). The plasma emission spectrum recorded at a contrast of 10^8 was found to be markedly different from the spectrum recorded earlier for a contrast of 10^2-10^6: it differed mainly in that the spectral transitions in relatively low-charged ions (B-, C-, N-, O-, and F-like ions) were suppressed, and transitions in He-like argon were enhanced. This spectrum behavior was similar to that observed earlier when the contrast was raised from 10^2 to 10^6 [72, 133, 138]. However, certain new spectral structures, which are denoted as transitions in hollow ions in Figs 20b and 21a, now became apparent in the vicinity of the K_α and He_β lines. On raising the laser contrast to 10^{10}, the intensity of these structures rose significantly, as did the intensities of He-like lines.

In the second series of experiments, the laser contrast was fixed at the value of 10^{10}, and the laser pulse duration was varied (Fig. 21b). With increasing pulse duration, the total intensity of the spectra near the argon He_α line was found to decrease, while the relative intensity of transitions in hollow ions became higher. This behavior of hollow ion spectra seems to be quite natural, because the lengthening of the main pulse also implies a rise in the laser contrast, with the difference that we are dealing with an energy contrast rather than a power contrast ratio. To state it in different terms, for a fixed value of the power contrast ratio, increasing the main pulse duration leads to a relative lowering of the prepulse energy. As a result, the prepulse exerts a substantially weaker effect on the cluster target, and the emission spectra are formed primarily at the stage of femtosecond pulse interaction with the cool dense substance.

It was shown recently in Ref. [105] that the main spectral features observable in Fig. 21a are formed at different stages of plasma evolution.

The spectra of hollow ions are emitted at the first moments (for several femtoseconds) of interaction of the main laser pulse with clusters. At this time, the plasma temperature ranges 10–20 eV, the electron density varies in the $10^{22}-10^{23}$ cm^{-3} range, and a hot electron component is present.

Radiated somewhat later (several dozen or hundred femtoseconds later) are the more usual dielectronic satellites which arise from transitions in Li- to O-like ions, and Rydberg transitions in He-like ions. By this time, the electron temperature rises to 100–500 eV, and the electron density lowers to the values of $10^{21}-10^{22}$ cm^{-3}. The influence of hot electrons still remains quite significant.

At a later time (~ 1 ps), the thermalization of hot electrons brings the electron temperature to about 1 keV, the electron density lowers to values on the order of 10^{20} cm^{-3}, and the plasma emits primarily the ordinary spectral lines of multiply charged ions, the resonance and intercombination lines of Ar XVII in particular. We note that this scenario also follows from the results obtained earlier in Refs [72, 104, 123].

The ion emission spectra calculated in the framework of the model described above were compared with observations

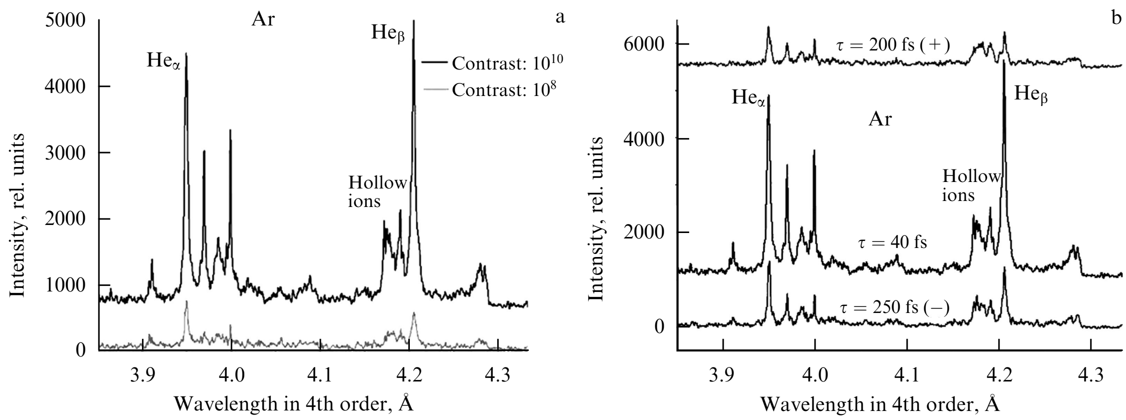

Figure 21. (a) Variation of observed spectra upon variation of the laser contrast. (b) Variation of the spectra upon variation of laser pulse duration [105].

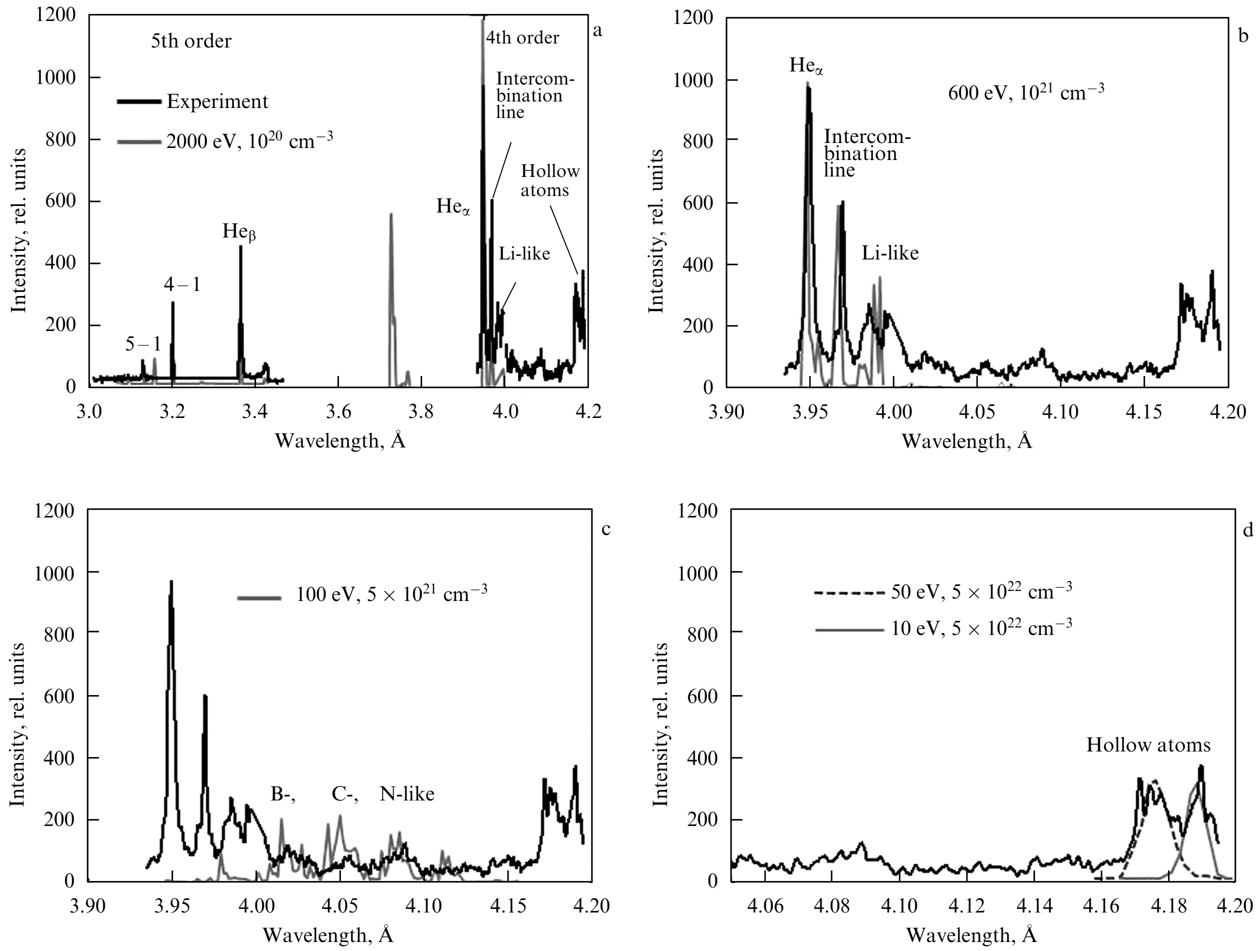

Figure 22. Comparison of calculated spectra with observations. In the calculations, the concentration of the hot electron component with an average energy of 7 keV was assumed to be equal to 1% of the total plasma electron density and invariable with time [105]. The dark curves fit experimental data, the grey and dashed ones stand for the calculated data.

in Fig. 22. It was assumed in the calculations that the concentration of the hot electron component with an average energy of 7 keV is equal to 1% of the total plasma electron density and is invariable in time. Obviously, this assumption is unrealistic; however, test calculations showed that variations of the hot electron fraction do not change the main spectral features, though they affect the calculated spectra [104].

Figure 22a gives the result of ATOMIC–FS calculations at a temperature of 2000 eV and an electron number density of 10^{20} cm^{-3}. At this temperature, the argon plasma consists primarily of H- and He-like ions, and the He$_\alpha$, He$_\beta$, He$_\gamma$, and He$_\delta$ lines of the resonance series are easily identified. One can see from this figure that the relative intensity of Rydberg transitions is somewhat higher in experiment than in the theory. This may well be due to the uncertainty in crystal reflectivities in different orders (it will be recalled that some lines were observed in the fifth reflection order, and some in the fourth one). The calculated results also predict a strong line around $\lambda = 3.72$ Å, but no measurements were made in this region.

Figure 22b presents the results of ATOMIC–FS spectrum calculations in the range between the He$_\alpha$ and K$_\alpha$ lines (i.e. in the 3.90–4.20 Å wavelength range) at a somewhat lower temperature (600 eV) and a higher electron number density (10^{21} cm^{-3}). At this temperature, the argon plasma contains primarily He-like Ar XVII ions, and we see a nice agreement between the theory and experiment for the lines of these ions, and a good agreement for lithium dielectronic satellites.

Figure 22c depicts the results of ATOMIC–MUTA calculations for $T_e = 100$ eV and $N_e = 5 \times 10^{21}$ cm^{-3}. At this temperature, lower-charge states of argon ions, primarily Be-, B-, C-, and N-like, dominate the plasma. The spectral peaks predicted by the calculation are identified as the 2p–1s transitions in these ions and correlate well with the spectra observed in the 4th order of reflection.

Lastly, Fig. 22d shows the data of two ATOMIC–MUTA calculations made for the same electron number density, 5×10^{22} cm^{-3}, and temperatures of 10 and 50 eV. The argon plasma is now dominated by almost neutral ions (the neutral Ar I at a temperature of 10 eV, and Ar VI, Ar VII at 50 eV). At these temperatures, the thermal electrons can excite only the valence shells of these ions, whose radiative decay does not produce X-ray photons. However, a hot electron fraction can ionize electrons from the inner K shell and thereby excite the states of hollow low-charged argon ions. The radiation of such hollow states for all ions, from Ar I to Ar VIII, will lie in the 4.15–4.20 Å wavelength range. With reference to Fig. 22d, the experimental spectrum in this wavelength range is reproduced by model calculations quite well, which proves the presence of hollow ions in the plasma under consideration. To exemplify the state of a hollow ion which makes a

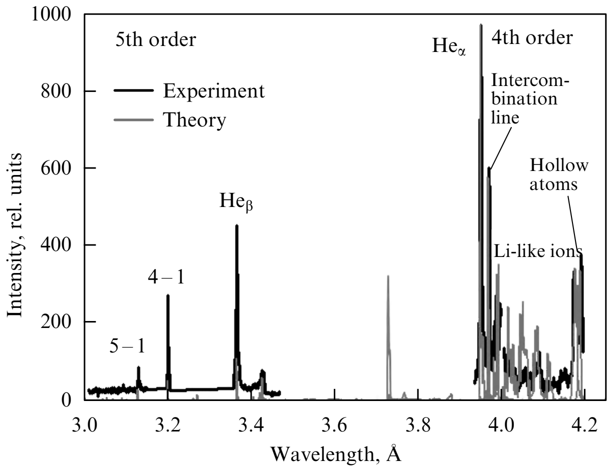

Figure 23. Model spectra calculated taking into account the scenario of laser-cluster plasma evolution and experimental spectra recorded in the 4th and 5th crystal reflection orders for a laser pulse duration of 40 fs and an ultrahigh laser contrast (10^{10}) [105]. Dark curves fit the experimental data, and the grey curve mark the calculated results.

contribution to the observed spectrum, we mention the configuration $1s^12s^22p^63s^23p^43d^24f^1$, which decays to the state $1s^22s^22p^53s^23p^43d^24f^1$ giving birth to a spectral line with $\lambda = 4.185$ Å. In reality, the majority of configurations that make contributions to the emission spectrum are related to the additional excitation of two or more valence electrons and their transition to the 3d, 4l, or 5l subshells, i.e. to the hollow ions not only of the KL type, but also of the types KLM, KLM^2, etc. At the same time, the excitation of K^2 hollow ions was not observed in the plasma under study.

The main outcome of the research conducted in Ref. [105] actually is that an adequate description of the emission spectra of plasma generated in the interaction of high-power femtosecond laser pulses with micrometer- and submicrometer-sized clusters is impossible, first, without including the hot electron fraction and, second, without considering in sufficient detail the variety of ion states, comprising different types of hollow ion states. For instance, the model spectra calculated with regard to the factors listed above and the scenario of laser-cluster plasma evolution are represented in Fig. 23. Also shown there are the experimental spectra recorded in the 4th and 5th crystal reflection orders for a laser pulse duration of 40 fs and an ultrahigh laser contrast (10^{10}). As is easily seen, throughout the 3.0–4.2 Å wavelength range the spectra agree nicely as regards the positions of all significant observable features and their intensities.

Of course, the above-described model is quite coarse in some respects. First of all, we would like to see it taking into account the time dependences of the populations of different ion states and of the free-electron energy distribution function of the plasma. The former calls for the employment of time-dependent collisional-radiative kinetic equations, and the latter necessitates the solution of the Boltzmann kinetic equation for free electrons with the inclusion of ionization and recombination processes. The authors of Ref. [105] intend to develop their model along these lines.

4.2.3. Hollow oxygen ions in the interaction of a picosecond laser pulse with a solid target. The spectra of hollow oxygen ions were recently discovered by Colgan et al. [106] in the course of an investigation aimed at developing the methods of diagnostics from the wing shapes of X-ray spectral lines. In the spectra of a mylar target, they observed spectral structures in the 20–21 Å wavelength range, which were impossible to ascribe to any of the known radiative transitions in oxygen ions. Initially the authors of Ref. [106] hypothesized that those structures arose from the high-Z impurity elements contained in the target, but detailed spectral studies proved that those structures arose from transitions in KL hollow oxygen ions. Gas dynamics simulations performed in Ref. [106] allowed specifying the plasma regions responsible for the emission of hollow ion spectra.

The experiments were performed on the COmpact Multipulse Terawatt (COMET) laser at Lawrence Livermore National Laboratory (USA) [144]. This laser could generate pulses at the fundamental (1054 nm) or doubled (527 nm) frequency ranging from 500 fs to 600 ps in duration [145]. In the experiments discussed below, advantage was taken of the second harmonic, and the pulse duration was equal to 250 ps at an energy of 5 J. The laser radiation was focused with an off-axis parabolic mirror ($f/4.8$) with a focal length of 30 cm. The peak intensity of 5×10^{15} W cm^{-2} was achieved for a focal spot diameter of less than 20 μm. The targets were 1.5- and 3-μm-thick mylar ($C_{10}H_8O_4$) foils, as well as 300-μm-thick disks 1.4 mm in diameter made of SiO_2 aerogel with a density of 50 mg cm^{-3}

X-ray plasma emission spectra were recorded with a spectrometer equipped with a varied line space grating (2400 lines per millimeter, on average) with a radius of curvature of 44.3 m [144]. The use of a 10- or 25-μm-wide additional slit enabled observing spatially resolved spectra. The spectra were recorded with a PI-SX X-ray CCD camera cooled with liquid nitrogen. The CCD matrix contained 1340×1300 pixels for a cell size of 20×20 μm^2; the signal-to-noise ratio was no less than 5000 in a spectrum recorded in one shot. The spectrometer viewed the target surface at a grazing angle of 5°, thereby lowering the Doppler shifts due to plasma expansion to about 2 mÅ.

Figure 24 demonstrates the typical spectrum of a mylar target in the 15–23 Å wavelength range. The majority of observed spectral lines are readily identified as the resonance series of H- and He-like ions of oxygen and their dielectronic satellites. Only a part of the spectrum was incomprehensible in the 20–21 Å wavelength range, which turned out to belong to hollow ions.

To find this out, computations were made using the codes of Los Alamos National Laboratory mentioned above (the CATS, GIPPER, and ATOMIC codes). The atomic model comprised almost 10,000 energy levels, with the inclusion of hollow ion states [106]. For the H-like ion, account was taken of all nl levels up to $n = 7$; for the He-like ion, included were all $1s^2$, $1snl$, and $2lnl'$ levels with $n < 7$, as well as $2l^2$ and $3l^2$; for the Li-like ion, the configurations $1s^2nl$, $1s2l^2$, $1s2lnl'$, $1s3l^2$, $2l^3$, and $2l^2nl'$ with $n < 5$; for the Be-like ion, the configurations $1s^22l^2$, $1s^22lnl'$, $1s^23l^2$, $1s2l^3$, $1s2l^2nl'$, $1s3l^3$, $2l^4$, and $2l^3nl$ with $n < 5$, and for the B-like ion, the configurations $1s^22l^3$, $1s^22l^2nl'$, $1s^22l3l'^2$, $1s2l^3nl'$, $1s2l^4$, $1s2l3l'^3$, $2l^5$, and $2l^4nl$ with $n < 5$. The system of stationary kinetic equations was solved.

The spectra modelled for $T_e = 150$ eV and $N_e = 3.6 \times 10^{20}$ cm^{-3} reproduced the observed spectrum reasonably well throughout the wavelength range, with the exception of the 20–21 Å interval, where they uncovered any spectral lines. The lines show up in this region only in a significantly higher density plasma with an appreciably lower temperature, for

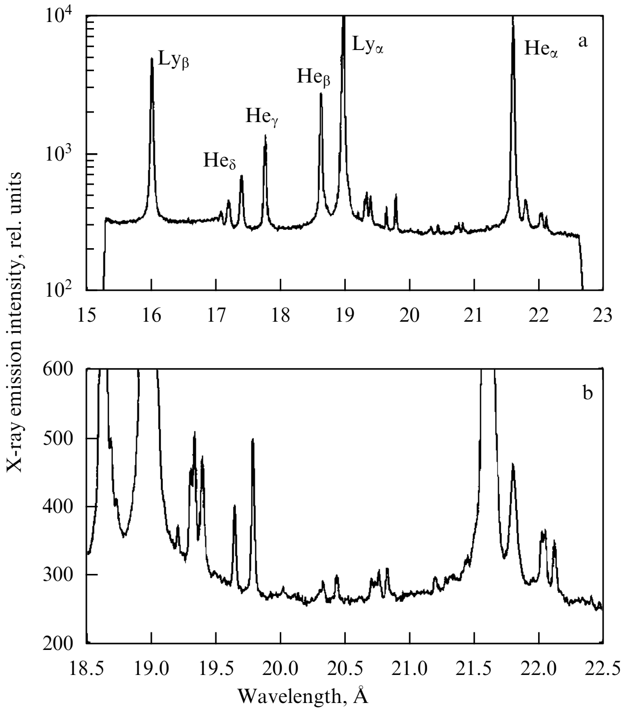

Figure 24. Emission spectra of mylar foil observed in Ref. [106]: (a) panoramic spectrum in the wavelength range 15.3–22.6 Å, and (b) portion of the spectrum in the wavelength range 18.5–22.5 Å.

instance, at $T_e = 60$ eV and $N_e = 5 \times 10^{22}$ cm^{-3}. Under these plasma parameters, the 3–1 transitions in Be-like oxygen ($1s2p^23p - 1s^22p^2$ type transitions) turn out to be rather intense in the 20.0–20.5 Å wavelength range, and similar lines of B-like oxygen are emitted in the $\lambda = (20.5-20.8)$ Å range. The highly exotic $1s2p5d - 1s^24d$ type transitions of Li-like oxygen turn out to make a contribution at wavelengths close to 21 Å. Therefore, the simulation data suggest that the groups of spectral transitions recorded in the 20–21 Å wavelength range comprise transitions in KL hollow ions.

It is pertinent to note that no spectral lines were observed in the 20–21 Å wavelength range in experiments on the aerogel target. This conclusion is also borne out by the modeling data. In the case of the aerogel target, the highest plasma density may amount to only $N_e = 1.5 \times 10^{22}$ cm^{-3}, even if all the atoms of oxygen and silicon are ionized to the state of bare nuclei. Since the degree of ionization under the temperatures involved will be much lower, especially for silicon ions, the real plasma density will prove to be even lower. By contrast, the density might be as high as 4×10^{24} cm^{-3} for a completely ionized mylar target, and therefore the average value of 5×10^{22} cm^{-3} required for agreement between the calculated and experimental data seems to be quite reasonable in this case.

The inferences made in Ref. [106] about formation of the plasma emission spectrum may be formulated as follows. The major part of the radiation is emitted by relatively hot and moderately dense plasma regions with $T_e = 100-150$ eV and $N_e = 3.6 \times 10^{20}$ cm^{-3}. A small part of the radiation arising from radiative transitions in hollow ions is emitted by cooler higher-density plasma regions which may surround the central spot. Since the spectra of hollow ions may be located in the spectral regions devoid of ordinary ion lines, they may well be discovered, despite their small total energy. In the framework of these notions, a synthetic spectrum was calculated in Ref. [106] assuming that the dense region amounts to only 1% of the total plasma domain. It turned out that the model spectrum by and large was in satisfactory agreement with the experimental one. However, its drawbacks, which in fact are typical for the modelled spectra of hollow ions, were also manifested. Specifically, the precision of calculating the wavelengths of hollow ion transitions to date is significantly inferior to that for the wavelengths of ordinary spectral lines, including satellites. Of course, this is largely due to the complexity of calculating the energy structure of states with a large number of open shells. However, this is at least partially also due to the fact that such computations had not been conducted at all until recently, and therefore attempts to adapt the existing program packages to the specific case of hollow ion configurations have actually not been undertaken. It is valid to state that the present-day uncertainty of hollow-ion spectrum calculations is on the order of (1–0.1)%, ranking approximately 1–2 orders of magnitude below the accuracy of ordinary spectrum calculations. The only exception is provided by the hollow two-electron configurations of He-like ions, for which the uncertainty of calculations is the same as for satellite transitions.

For verifying the hypothesis that two plasma domains with radically different parameters are responsible for the radiation, gas dynamics simulations was undertaken in Ref. [106]. To this end, advantage was taken of the Hydra two-dimensional radiative gas dynamics program [146]. According to these simulations, for $t = 500$ ps (the peak of laser intensity corresponded to the point in time $t_0 = 287$ ps) the central part of the target surface 30–40 μm in diameter is rather hot (several hundred electron-volts) and moderately dense, while the outer regions are substantially cooler (several dozen electron-volts), but retain the near-solid-state density. At later times, ~ 1 ns, the plasma cools down rapidly to a temperature on the order of 40 eV even in the focal spot region. It is precisely the dense plasma regions located at distances of 30–100 μm from the center of the focal spot that are responsible for the emission of hollow ion spectra. Therefore, the data of gas dynamics simulations are entirely consistent with the model employed in the computation of emission spectra.

5. Conclusions

To date, many observations have been made of such exotic atomic objects as hollow ions. We see that their spectra are excited in the interaction of ultrashort high-power laser pulses with condensed targets (solid targets, clusters) and even dense gases (see, for instance, Refs [86, 147, 148]). In this sense, the spectra of hollow ions are no longer exotic and are a relatively widespread physical object. The fact that their excitation is especially efficient in high-density plasmas permits, broadly speaking, developing X-ray spectral techniques for ultrahigh-density plasma diagnostics [7, 8, 42–44].

It is highly significant that such spectra must be excited in warm dense matter [7, 8, 38–49] and in nonideal plasmas [42, 43, 50, 51]. For instance, in work [103] they were recorded in plasma nonideal in ion–ion interactions and weakly nonideal in electron–ion interactions. An important point is that the nonideality effects will hardly affect the hollow-ion spectra themselves, even though they may be emitted from a nonideal plasma: they are emitted in the electron transitions between deep-lying inner shells of ions. This signifies that X-ray techniques based on detecting these spectra may be validly applied for diagnosing nonideal plasmas. By contrast, the application of techniques reliant on the spectral transitions between the outer shells of ions calls for a reconsideration of the existing collisional-radiative kinetic plasma models and, perhaps, for a new theory of the spectra of a strongly nonideal plasma [7, 8, 42–44], which will undoubtedly take a long time to develop.

The spectra of hollow ions will gain in importance progressively with advancements in the area of the development and employment of both the plasma X-ray lasers (see, for instance, Refs [149–151]) and X-ray free-electron lasers. In recent years, three of them, specifically, FLASH (Free-electron LASer in Hamburg) (Germany), LCLS (SLAC National Accelerator Laboratory) (USA), and SCSS [Spring-8 Compact SASE (Self-Amplified Spontaneous Emission) Source] (Japan), have been actively used to study the interaction of high-power short-wavelength radiation with matter (see, for instance, Refs [152–182]). And it is not even a matter of the feasibility of using the states of hollow ions to obtain laser action in the X-ray region (see, for example, Refs [183, 184]); rather it is a matter of the basic features of the interaction of high-power X-ray laser radiation with matter. In the experiments of this kind, the inner-shell ionization processes in atoms and ions, which are responsible for the production of hollow ions, are the principal mechanism of laser energy absorption, irrespective of whether the X-ray laser radiation source is a plasma laser or a free-electron laser. In this case, the resultant substance state will be characterized by solid-state density and relatively low temperatures, i.e., will be a nonideal plasma in many instances [7, 8, 42–44], with only few reliable techniques appropriate for determining its parameters.

In our view, realizing the diagnostic capabilities of hollow-ion spectra (like those of any other, incidentally) calls for the further development of techniques for calculating atomic structures with a large number of open electron shells. Only upon the attainment of spectroscopic precision of these calculations (with a relative uncertainty of about 10^{-4}) will it be possible to classify with confidence the spectra of hollow ions and ascribe them not only to a certain charge state, but also to one electron configuration or another and, in individual cases, to fine-structure levels. Developing the methods of computation, in turn, requires experimental information about the spectra of such ions, which brings up the task of carrying out systematic experimental research in this area.

In essence, the situation bears resemblance to that with satellite spectra, encountered in the second half of the past century. When the significance of such spectra for practical applications was realized, the precision of satellite structure calculations was quite insufficient. In one or two decades, however, different theoretical groups developed alternative approaches (relativistic perturbation theory, multiconfiguration Hartree–Fock methods with relativistic corrections, Dirac–Fock methods, the semiempirical relativistic model potential approach) which enabled obtaining the requisite data with the accuracy required for experiments. This, in turn, lent impetus to the development of X-ray spectral diagnostic techniques, which came to be usefully employed for rarefied astrophysical and dense laboratory plasmas. Such a step should now be taken in relation to the spectra of hollow ions.

Acknowledgments. This work was supported by the Russian Foundation for Basic Research under grant Nos 10-02-91174-GFEN-a, 10-02-00345-a, and 10-07-00227-a.

References

1. Presnyakov L P *Usp. Fiz. Nauk* **119** 49 (1976) [*Sov. Phys. Usp.* **19** 387 (1976)]
2. Boiko V A et al. *Rentgenovskaya Spektroskopiya Lazernoi Plazmy* (X-Ray Spectroscopy of Laser Plasma) (Itogi Nauki i Tekhniki (Advances in Science and Technology), Ser. Radiotekhnika (Ser. Radio Engineering, Vol. 27, Ed. N G Basov) (Moscow: VINITI, 1980)
3. Boiko V A et al. *J. Sov. Laser Res.* **6** (2) 83 (1985)
4. Aglitskii E V, Safronova U I *Spektroskopiya Avtoionizatsionnykh Sostoyanii Atomnykh Sistem* (Spectroscopy of Autoionization States of Atomic Systems) (Moscow: Energoatomizdat, 1985)
5. Boiko V A, Pal'chikov V G, Skobelev I Yu, Faenov A Ya *Rentgenovskaya Spektroskopiya Mnogozaryadnykh Ionov* (X-Ray Spectroscopy of Multiply Charged Ions) (Moscow: Energoatomizdat, 1988)
6. Skobelev I Yu et al. *Zh. Eksp. Teor. Fiz.* **108** 1263 (1995) [*JETP* **81** 692 (1995)]
7. Fortov V E *Usp. Fiz. Nauk* **179** 653 (2009) [*Phys. Usp.* **52** 615 (2009)]
8. Fortov V E *Ekstremal'nye Sostoyaniya Veshchestva na Zemle i v Kosmose* (Extreme States of Matter on Earth and in the Cosmos) (Moscow: Fizmatlit, 2008) [Translated into English (Berlin: Springer, 2011)]
9. Faenov A Ya et al. *Phys. Rev. A* **51** 3529 (1995)
10. Renner O et al. *J. Quantit. Spectrosc. Radiat. Transfer* **71** 623 (2001)
11. Eidmann K et al. *J. Quantit. Spectrosc. Radiat. Transfer* **65** 173 (2000)
12. Eidmann K et al. *J. Quantit. Spectrosc. Radiat. Transfer* **81** 133 (2003)
13. Saemann A et al. *Phys. Rev. Lett.* **82** 4843 (1999)
14. Rosmej F B et al. *J. Quantit. Spectrosc. Radiat. Transfer* **65** 477 (2000)
15. Fournier K B et al. *Phys. Rev. E* **70** 016406 (2004)
16. Chen S N et al. *Phys. Plasmas* **16** 062701 (2009)
17. Auguste T et al. *Pis'ma Zh. Eksp. Teor. Fiz.* **72** 54 (2000) [*JETP Lett.* **72** 38 (2000)]
18. Skobelev I Yu et al. *Zh. Eksp. Teor. Fiz.* **121** 88 (2002) [*JETP* **94** 73 (2002)]
19. Abdallah J (Jr.) et al. *J. Quantit. Spectrosc. Radiat. Transfer* **62** 1 (1999)
20. Coté C Y, Kieffer J C, Peyrusse O *Phys. Rev. E.* **56** 992 (1997)
21. Uschmann I et al. *Laser Part. Beams* **17** 671 (1999)
22. Bastiani-Ceccotti S et al. *High Energy Density Phys.* **6** 99 (2010)
23. Faenov A Y et al. *Proc. SPIE* **3157** 10 (1997)
24. Urnov A M et al. *Pis'ma Zh. Eksp. Teor. Fiz.* **67** 467 (1998) [*JETP Lett.* **67** 489 (1998)]
25. Faenov A Ya et al. *Phys. Scripta* **T80** 536 (1999)
26. Maksimchuk A et al. *J. Quantit. Spectrosc. Radiat. Transfer* **65** 367 (2000)
27. Briand J-P et al. *Phys. Rev. Lett.* **65** 159 (1990)
28. Bailey J et al. *Lasers Part. Beams* **8** 555 (1990)
29. Limburg J et al. *Phys. Rev. Lett.* **75** 217 (1995)
30. Briand J-P et al. *Phys. Rev. A* **54** 4136 (1996)
31. Ninomiya S et al. *Phys. Rev. Lett.* **78** 4557 (1997)
32. Briand J-P et al. *Phys. Rev. A* **55** 3947 (1997)
33. Winter H, Aumayr F *J. Phys. B At. Mol. Opt. Phys.* **32** R39 (1999)
34. Schenkel T et al. *Prog. Surf. Sci.* **61** 23 (1999)
35. McMahon S J et al. *Phys. Rev. A* **83** 022901 (2011)
36. Rzadkiewicz J et al. *Phys. Rev. A* **82** 012703 (2010)
37. Diamant R et al. *Phys. Rev. Lett.* **84** 3278 (2000)
38. Diamant R et al. *Phys. Rev. A* **62** 052519 (2000)
39. Diamant R et al. *Phys. Rev. A* **63** 022508 (2001)
40. Diamant R et al. *Phys. Rev. Lett.* **91** 193001 (2003)
41. Aglitsky Y et al. *Phys. Plasmas* **3** 9 (1996)
42. Fortov V E *Ekstremal'nye Sostoyaniya Veshchestva* (Extreme States of Matter) (Moscow: Fizmatlit, 2009)
43. Fortov V E, Khrapak A G, Yakubov I T *Fizika Neideal'noi Plazmy* (Physics of Nonideal Plasma) (Moscow: Fizmatlit, 2004)

44. Fortov V, Iakubov I, Khrapak A *Physics of Strongly Coupled Plasma* (Oxford: Oxford Univ. Press, 2006)
45. Rosmej F B et al. *J. Phys. Conf. Ser.* **72** 012007 (2007)
46. Fäustlin R R et al. *Phys. Rev. Lett.* **104** 125002 (2010)
47. Norman G E, Skobelev I Yu, Stegailov V V, in *4-ya Vserossiiskaya Shkola-Seminar "Aerofizika i Fizicheskaya Mekhanika Klassicheskikh i Kvantovykh Sistem", AFM-2010* (Proceedings of the 4th All-Russian Workshop "Aerophysics and Physical Mechanics of Classical and Quantum Systems APhM-2010") (Moscow: Institute for Problems in Mechanics, RAS, 2011)
48. Norman G E, Skobelev I Yu, Stegailov V V, in *XXV Intern. Conf. on Equation of State for Matter, March 1 – 6, 2010, Elbrus, Russia. Book of Abstracts*
49. Norman G E, Skobelev I Yu, Stegailov V V *Contrib. Plasma Phys.* **51** 411 (2011)
50. Rosmej F B et al. *J. Quantit. Spectrosc. Radiat. Transfer* **81** 395 (2003)
51. Starostin A N, Iosilevskii I L (Exec. Eds) *Entsiklopediya Nizkotemperaturnoi Plazmy* (Encyclopedia of Low-Temperature Plasma) (Ed.-in-Chief V E Fortov) Ser. B *Spravochnye Prilozheniya, Bazy i Banki Dannykh* (Reference Data and Data Bases) Vol. 1 *Termodinamicheskie Svoistva Nizkotemperaturnoi Plazmy* (Thermodynamic Properties of Low-Temperature Plasma) (Moscow: Fizmatlit, 2004)
52. Rosmej F B et al. *Pis'ma Zh. Eksp. Teor. Fiz.* **65** 679 (1997) [*JETP Lett.* **65** 708 (1997)]
53. Rosmej F B et al. *J. Quantit. Spectrosc. Radiat. Transfer* **58** 859 (1997)
54. Rosmej F B et al. *Phys. Rev. E* **66** 056402 (2002)
55. Abdallah J et al. *Kvantovaya Elektron.* **20** 1159 (1993) [*Quantum Electron.* **23** 1005 (1993)]
56. Khakhalin S Ya et al. *Phys. Scripta* **50** 102 (1994)
57. Khakhalin S Ya et al. *Zh. Eksp. Teor. Fiz.* **105** 1181 (1994) [*JETP* **78** 633 (1994)]
58. Nilsen J et al. *Izmerit. Tekh.* (5) 3 (1994)
59. Osterheld A L et al. *AIP Conf. Proc.* **332** 215 (1995); Preprint UCRL-JC-117928 (1994)
60. Faenov A Ya et al. *Phys. Scripta* **51** 454 (1995)
61. Skobelev I Yu et al. *Phys. Rev. E* **55** 3773 (1997)
62. Skobelev I Yu et al. *Kvantovaya Elektron.* **25** 697 (1998) [*Quantum Electron.* **28** 677 (1998)]
63. Rosmej F B et al. *J. Phys. B At. Mol. Opt. Phys.* **31** L921 (1998)
64. Rosmej F B et al. *Phys. Rev. A* **63** 063409 (2001)
65. Rosmej F B et al. *J. Quantit. Spectrosc. Radiat. Transfer* **71** 639 (2001)
66. Abdallah J et al. *Kvantovaya Elektron.* **30** 694 (2000) [*Quantum Electron.* 30 694 (2000)]
67. Vainshtein L A, Safronova U I, Preprint No. 1 (Troitsk: Institute of Spectroscopy, USSR Academy of Sciences, 1985)
68. Vainshtein L A, Safronova U I, in *Korrelyatsionnye i Relyativistskie Effekty v Atomakh i Ionakh* (Correlation and Relativistic Effects in Atoms and Ions) (Ed. U I Safronova) (Moscow: AN SSSR, Otd. Obshch. Fiz. i Astron. Nauchnyi Sovet po Spektroskopii, 1986) p. 190
69. Abdallah J (Jr.) et al. *Phys. Rev. A* **63** 032706 (2001)
70. Zhidkov A G et al. *Phys. Plasma* **8** 3718 (2001)
71. Hansen S B et al. *Phys. Rev. E* **66** 046412 (2002)
72. Abdallah J (Jr.) et al. *Phys. Rev. A* **68** 063201 (2003)
73. Auguste T et al. *J. Quantit. Spectrosc. Radiat. Transfer* **71** 147 (2001)
74. Fournier K B et al. *Phys. Rev. E* **67** 016402 (2003)
75. Moribayashi K, Sasaki A, Zhidkov A *Phys. Scripta* **T92** 185 (2001)
76. Gitomer S J et al. *Phys. Fluids* **29** 2679 (1986)
77. Zhidkov A et al. *Phys. Rev. E* **62** 7232 (2000)
78. Geloni G et al. *New J. Phys.* **12** 035021 (2010)
79. Togashi T et al. *Opt. Express* **19** 317 (2011)
80. Doumy G et al. *Phys. Rev. Lett.* **106** 083002 (2011)
81. Nagler B et al. *Nature Phys.* **5** 693 (2009)
82. Young L et al. *Nature* **466** 56 (2010)
83. Rosmej F B, Lee R W *Europhys. Lett.* **77** 24001 (2007)
84. McPherson A et al. *Nature* **370** 631 (1994)
85. McPherson A et al. *Phys. Rev. Lett.* **72** 1810 (1994)
86. Rosmej F B et al. *J. Phys. B At. Mol. Opt. Phys.* **32** L107 (1999)
87. Eissner W, Jones M, Nussbaumer H *Comput. Phys. Commun.* **8** 270 (1974)
88. Faucher P, Dubau J *Phys. Rev. A* **31** 3672 (1985)
89. Inal M K, Dubau J *J. Phys. B At. Mol. Opt. Phys.* **22** 3329 (1989)
90. Bollanti S et al. *Nuovo Cimento D* **18** 1241 (1996)
91. Young B K F et al. *Rev. Sci. Instrum.* **69** 4049 (1998)
92. Abdallah J (Jr.), Clark R E H, Cowan R D, Report LA-11436-M Vol. 1 (Los-Alamos: LANL, 1988)
93. Colgan J et al. *Phys. Scripta* **78** 015302 (2008)
94. Faenov A Ya et al. *J. Phys. Conf. Ser.* **163** 012016 (2009)
95. Faenov A Ya et al. *J. Plasma Fusion Res. SERIES* **8** 1210 (2009)
96. Ammosov M V, Delone N B, Krainov V P *Zh. Eksp. Teor. Fiz.* **91** 2008 (1986) [*Sov. Phys. JETP* **64** 1191 (1986)]
97. Faenov A Ya et al. *Phys. Scr.* **50** 333 (1994)
98. Janev R K, Presnyakov L P, Shevelko V P *Physics of Highly Charged Ions* (Berlin: Springer-Verlag, 1985)
99. Ostrovsky V N *J. Phys. B At. Mol. Opt. Phys.* **28** 3901 (1995)
100. Rosmej F B, Lisitsa V S *Phys. Lett. A* **244** 401 (1998)
101. Boyer K, Rhodes C K *J. Phys. B At. Mol. Opt. Phys.* **27** L633 (1994)
102. Borisov A B et al. *J. Phys. B At. Mol. Opt. Phys.* **29** L43 (1996)
103. Gauthier J-C et al. *Phys. Rev. E* **52** 2963 (1995)
104. Colgan J et al. *Laser Part. Beams* **26** 83 (2008)
105. Colgan J et al. *High Energy Density Phys.* **7** 77 (2011)
106. Colgan J et al. *High Energy Density Phys.* **6** 295 (2010)
107. Ditmire T et al. *Phys. Rev. A* **53** 3379 (1996)
108. Tarasov M et al. *Pis'ma Zh. Eksp. Teor. Fiz.* **68** 426 (1998) [*JETP Lett.* **68** 454 (1998)]
109. Dobosz S et al. *Zh. Eksp. Teor. Fiz.* **115** 2051 (1999) [*JETP* **88** 1122 (1999)]
110. Parra E et al. *Phys. Rev. E* **62** R5931 (2000)
111. Stenz C et al. *Kvantovaya Elektron.* **30** 721 (2000) [*Quantum Electron.* **30** 721 (2000)]
112. Blasco F et al. *Rev. Sci. Instrum.* **72** 1956 (2001)
113. Hagena O F, Obert W *J. Chem. Phys.* **56** 1793 (1972)
114. Hagena O F *Surf. Sci.* **106** 101 (1981)
115. Hagena O F *Rev. Sci. Instrum.* **63** 2374 (1992)
116. Junkel-Vives G C et al. *Phys. Rev. E* **65** 036410 (2002)
117. Boldarev A S et al. *Pis'ma Zh. Eksp. Teor. Fiz.* **73** 583 (2001) [*JETP Lett.* **73** 514 (2001)]
118. Boldarev A S, Gasilov V A *Mat. Modelirovanie* **15** (3) 55 (2003)
119. Boldarev A et al. *Proc. SPIE* **5228** 446 (2003)
120. Skobelev I Yu et al. *Zh. Eksp. Teor. Fiz.* **121** 1124 (2002) [*JETP* **94** 966 (2002)]
121. Boldarev A S, Gasilov V A, Faenov A Ya *Pis'ma Zh. Tekh. Fiz.* **74** (4) 10 (2004) [*Tech. Phys. Lett.* **49** 388 (2004)]
122. Boldarev A S et al. *Rev. Sci. Instrum.* **77** 083112 (2006)
123. Sherrill M E et al. *Phys. Rev. E* **73** 066404 (2006)
124. Symes D R et al. *Phys. Rev. Lett.* **98** 123401 (2007)
125. Junkel-Vives G C et al. *Phys Rev. A* **64** 021201(R) (2001)
126. Junkel-Vives G C et al. *Phys. Rev. A* **66** 033204 (2002)
127. Davis J, Petrov G M, Velikovich A *Phys. Plasmas* **14** 060701 (2007)
128. Faenov A Ya et al. *Laser Part. Beams* **25** 267 (2007)
129. Nishikawa T et al. *Appl. Phys. B* **78** 885 (2004)
130. Sumeruk H A et al. *Phys. Rev. Lett.* **98** 045001 (2007)
131. Ditmire T et al. *J. Phys. B At. Mol. Opt. Phys.* **31** 2825 (1998)
132. Dobosz S et al. *Pis'ma Zh. Eksp. Teor. Fiz.* **68** 454 (1998) [*JETP Lett.* **68** 485 (1998)]
133. Fukuda Y et al. *Laser Part. Beams* **22** 215 (2004)
134. Smirnov B M *Clusters and Small Particles: in Gases and Plasmas* (New York: Springer, 2000)
135. Pikuz T A et al. *Appl. Opt.* **48** 6271 (2009)
136. Magunov A I et al. *Laser Part. Beams* **21** 73 (2003)
137. Kim K Y et al. *Phys. Rev. E* **73** 066403 (2006)
138. Fukuda Y et al. *Pis'ma Zh. Eksp. Teor. Fiz.* **78** 146 (2003) [*JETP Lett.* **78** 115 (2003)]
139. Faenov A Y et al. *Proc. SPIE* **4504** 121 (2001)
140. Cowan R D *The Theory of Atomic Structure and Spectra* (Berkeley: Univ. of California Press, 1981)
141. Clark R E H, Abdallah J (Jr.), Mann J B *Astrophys. J.* **381** 597 (1991)
142. Magee N H et al. *AIP Conf. Proc.* **730** 168 (2004)
143. Colgan J et al. *J. Phys. B At. Mol. Opt. Phys.* **43** 144021 (2010)
144. Dunn J et al. *Rev. Sci. Instrum.* **79** 10E314 (2008)
145. Dunn J et al. *Phys. Rev. Lett.* **84** 4834 (2000)
146. Marinak M M et al. *Phys. Plasmas* **5** 1125 (1998)
147. Rosmej F B et al. *Nucl. Instrum. Meth. Phys. Res. A* **464** 257 (2001)

148. Rosmej F B et al. *AIP Conf. Proc.* **506** 472 (2000)
149. Elton R C *X-Ray Lasers* (Boston: Academic Press, 1990)
150. London R, Matthews D, Suckewer S (Eds) *Applications of X-Ray Lasers* (Nat. Tech. Inform. Serv. Doc. No. LLNL-CONF-9206170) (San-Francisco, Nat. Tech. Inform. Serv. Doc., 1992)
151. Gasparyan P D, Starikov F A, Starostin A N *Usp. Fiz. Nauk* **168** 843 (1998) [*Phys. Usp.* **41** 761 (1988)]
152. Faenov A Ya et al. *Appl. Phys. Lett.* **94** 231107 (2009)
153. Alessi D et al. *Opt. Lett.* **35** 414 (2010)
154. Zimmer D et al. *Phys. Rev. A* **82** 013803 (2010)
155. Guilbaud O et al. *Opt. Lett.* **35** 1326 (2010)
156. Berrill M et al. *J. Opt. Soc. Am. B* **25** B32 (2008)
157. Suckewer S, Jaegle P *Laser Phys. Lett.* **6** 411 (2009)
158. Toleikis S et al. *High Energy Density Phys.* **6** 15 (2010)
159. Evans R G et al. *Appl. Phys. Lett.* **86** 191505 (2005)
160. Martins M et al. *Phys. Rev. A* **80** 023411 (2009)
161. Krikunova M et al. *New J. Phys.* **11** 123019 (2009)
162. Nelson A J et al. *Opt. Express* **17** 18271 (2009)
163. Vinko S M et al. *Phys. Rev. Lett.* **104** 225001 (2010)
164. Fang L et al. *Phys. Rev. Lett.* **105** 083005 (2010)
165. Cryan J P et al. *Phys. Rev. Lett.* **105** 083004 (2010)
166. Fäustlin R R et al. *Phys. Rev. Lett.* **104** 125002 (2010)
167. Jiang Y H et al. *Phys. Rev. A* **81** 051402(R) (2010)
168. Emma P et al. *Nature Photon.* **4** 641 (2010)
169. Seres J et al. *Nature Phys.* **6** 455 (2010)
170. Richter M et al. *J. Phys. B At. Mol. Opt. Phys.* **43** 194005 (2010)
171. Inubushi Y et al. *J. Phys. Conf. Ser.* **244** 022039 (2010)
172. Toleikis S et al. *J. Phys. B At. Mol. Opt. Phys.* **43** 194017 (2010)
173. Jiang Y H et al. *Phys. Rev. A* **82** 041403(R) (2010)
174. Hoener M et al. *Phys. Rev. Lett.* **104** 253002 (2010)
175. Epp S W et al. *J. Phys. B At. Mol. Opt. Phys.* **43** 194008 (2010)
176. Rosmej F B et al. *J. Phys. Conf. Ser.* **244** 042028 (2010)
177. McNeil B W J, Thompson N R *Nature Photon.* **4** 814 (2010)
178. Nilsen J, Scott H A *High Energy Density Phys.* **7** 6 (2011)
179. Giannessi L et al. *Phys. Rev. Lett.* **106** 144801 (2011)
180. Cederbaum L S et al. *Phys. Rev. Lett.* **106** 123001 (2011)
181. Galtier E et al *Phys. Rev. Lett.* **106** 164801 (2011)
182. Togashi T et al. *Opt. Express* **19** 317 (2011)
183. Moribayashi K, Sasaki A, Tajima T *Phys. Rev. A* **58** 2007 (1998)
184. Kim D-E et al. *Proc. SPIE* **5197** 229 (2003)